Supporting Information

Role of Hydrogen Bonding in Photoinduced Electron-Proton Transfer from Phenols to a Polypyridine Ru Complex with a Proton-Accepting Ligand

Sergei V. Lymar,* Mehmed Z. Ertem, Anna Lewandowska-Andralojc,† and Dmitry E. Polyansky*

lymar@bnl.gov, dep@bnl.gov

Chemistry Department, Brookhaven National Laboratory, Upton, New York 11973-5000, U.S.A.
† Present address: Faculty of Chemistry, Adam Mickiewicz University, Umultowska 89b, 61614, Poznan, Poland.

Table of Contents

Section S1

Derivations of the Stern-Volmer Dependencies for Time-Resolved and Steady-State Emission

Below, Scheme 1a (main text) is redrawn in a more complete form using simplified notations: P for phenol, S for solvent, $\mathbf{X}^*$ for Ru complex in its triplet excited state, and $\mathbf{X}P^*$ and $\mathbf{X}S^*$ for the hydrogen-bonded (HB) complexes between $\mathbf{X}^*$ and phenol and solvent, respectively. The ground state HB complexes are also included for completeness, even though the Uv-Vis absorption spectra of Ru complex **1** investigated in this work (Scheme 1, main text) show no evidence for the ground state H-bonding with phenols or trifluoroethanol (Figure S1).

Here, k_{nr} and k_{em} are the rate constants of the triplet state deactivations through non-radiative and radiative transitions, respectively, and k_{q} is the rate constant for the $\mathbf{X}P^*$ exited state quenching through a chemical reactions leading to products.

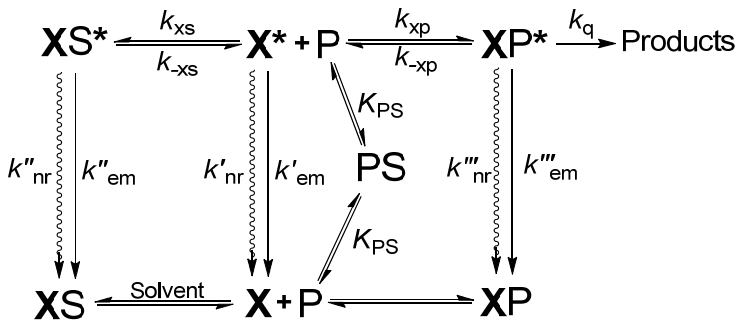

The hydrogen bonding equilibrium constants are defined as follows:

$$K_{\mathbf{X}\text{-P}} = \frac{k_{\mathrm{xp}}}{k_{\text{-xp}}} = \frac{[\mathbf{X}P^*]}{[\mathbf{X}^*][\mathrm{P}]} \qquad \text{(S1.1)}$$

$$K_{\mathbf{X}\text{-S}} = \frac{k_{\mathrm{xs}}}{k_{\text{-xs}}} = \frac{[\mathbf{X}S^*]}{[\mathbf{X}^*]} \qquad \text{(S1.2)}$$

$$K_{\mathrm{P\text{-}S}} = \frac{[\mathrm{PS}]}{[\mathrm{P}]} \qquad \text{(S1.3)}$$

Taking into account the very large excess of phenol over the total concentration of the excited complex, we have for the material balances

$$[\mathbf{X}^*_{\mathrm{T}}]=[\mathbf{X}^*] + [\mathbf{X}P^*] + [\mathbf{X}S^*] \qquad \text{(S1.4)}$$

and

$$[\mathrm{P_o}]=[\mathrm{P}] + [\mathrm{PS}] \qquad \text{(S1.5)}$$

Here, $[P_o]$ and $[\mathbf{X}_T^*]$ are the analytical concentration of added phenol and total concentration of excited complex, respectively. Correspondingly, [P] and $[\mathbf{X}^*]$ represent concentrations of the unbound (free) phenol and excited complex.

It is convenient to introduce the deactivation lifetimes for each of the excited Ru species

$$\tau_0^{\mathbf{X}} = \frac{1}{k_0^{\mathbf{X}}} = \frac{1}{k'_{\mathrm{nr}} + k'_{\mathrm{em}}} \tag{S1.6}$$

$$\tau_0^{\mathbf{X}\text{-S}} = \frac{1}{k_0^{\mathbf{X}\text{-S}}} = \frac{1}{k''_{\mathrm{nr}} + k''_{\mathrm{em}}} \tag{S1.7}$$

$$\tau_0^{\mathbf{X}\text{-P}} = \frac{1}{k_0^{\mathbf{X}\text{-P}}} = \frac{1}{k'''_{\mathrm{nr}} + k'''_{\mathrm{em}}} \tag{S1.8}$$

Note that the chemical reaction described by k_q is not included in the definition of $\tau_0^{\mathbf{X}\text{-P}}$.

Assuming the HB equilibrations to be rapid relative to all other exited state processes; that is,

$$k_{\mathrm{xp}}[P] + k_{\text{-xp}} \gg k_0^{\mathbf{X}} \quad \text{and} \quad k_{\mathrm{xp}}[P] + k_{\text{-xp}} \gg k_0^{\mathbf{X}\text{-P}} + k_q \tag{S1.9}$$

$$k_{\mathrm{xs}} + k_{\text{-xs}} \gg k_0^{\mathbf{X}} \quad \text{and} \quad k_{\mathrm{xs}} + k_{\text{-xs}} \gg k_0^{\mathbf{X}\text{-S}} \tag{S1.10}$$

and solving eq. S1.1-S1.5 we obtain the equilibrium distribution of all species in the scheme above

$$[P] = \frac{1}{1 + K_{\text{P-S}}}[P_o] \tag{S1.11}$$

$$[PS] = \frac{K_{\text{P-S}}}{1 + K_{\text{P-S}}}[P_o] \tag{S1.12}$$

$$[\mathbf{X}^*] = \frac{1 + K_{\text{P-S}}}{\left(1 + K_{\text{P-S}}\right)\left(1 + K_{\mathbf{X}\text{-S}}\right) + K_{\mathbf{X}\text{-P}}[P_o]}[\mathbf{X}_T^*] \tag{S1.13}$$

$$[\mathbf{X}S^*] = \frac{(1 + K_{\text{P-S}})K_{\mathbf{X}\text{-S}}}{\left(1 + K_{\text{P-S}}\right)\left(1 + K_{\mathbf{X}\text{-S}}\right) + K_{\mathbf{X}\text{-P}}[P_o]}[\mathbf{X}_T^*] \tag{S1.14}$$

$$[\mathbf{X}P^*] = \frac{K_{\mathbf{X}\text{-P}}[P_o]}{\left(1 + K_{\text{P-S}}\right)\left(1 + K_{\mathbf{X}\text{-S}}\right) + K_{\mathbf{X}\text{-P}}[P_o]}[\mathbf{X}_T^*] \tag{S1.15}$$

Note that under the conditions of rapid HB equilibration of the excited states (when the inequalities S1.9 and S1.10 are satisfied), the HB equilibria involving the ground states (**X**, **X**P, and **X**S in the Scheme above) become *inconsequential* for the distribution between the excited states.

Case I. Transient emission

The kinetics of the excited state decay following a pulsed excitation are described by

$$\frac{d[\mathbf{X}^*_{\mathrm{T}}]}{dt} = \frac{d[\mathbf{X}^*]}{dt} + \frac{d[\mathbf{X}\mathrm{S}^*]}{dt} + \frac{d[\mathbf{X}\mathrm{P}^*]}{dt} \tag{S1.16}$$

which expands to

$$-\frac{d[\mathbf{X}^*_{\mathrm{T}}]}{dt} = k_0^{\mathbf{X}}[\mathbf{X}^*] + k_0^{\mathbf{X}\text{-S}}[\mathbf{X}\mathrm{S}^*] + \left(k_0^{\mathbf{X}\text{-P}} + k_{\mathrm{q}}\right)[\mathbf{X}\mathrm{P}^*] \tag{S1.17}$$

Using eq. S1.13-S1.15, we obtain

$$-\frac{d[\mathbf{X}^*_{\mathrm{T}}]}{dt} = \frac{k_0^{\mathbf{X}}\left(1 + K_{\mathrm{P\text{-}S}}\right) + k_0^{\mathbf{X}\text{-S}}\left(1 + K_{\mathrm{P\text{-}S}}\right)K_{\mathbf{X}\text{-S}} + \left(k_0^{\mathbf{X}\text{-P}} + k_{\mathrm{q}}\right)K_{\mathbf{X}\text{-P}}[P_{\mathrm{o}}]}{\left(1 + K_{\mathrm{P\text{-}S}}\right)\left(1 + K_{\mathbf{X}\text{-S}}\right) + K_{\mathbf{X}\text{-P}}[\mathrm{P_o}]}\left[\mathbf{X}^*_{\mathrm{T}}\right] \tag{S1.18}$$

This equation describes a simple exponential decay

$$\left[\mathbf{X}^*_{\mathrm{T}}\right]_t = \left[\mathbf{X}^*_{\mathrm{T}}\right]_{t=0}\exp(-k_{\mathrm{obs}}t) \tag{S1.19}$$

with the observed rate constant, k_{obs}, and lifetime, τ_{obs}, given by

$$k_{\mathrm{obs}} = \frac{1}{\tau_{\mathrm{obs}}} = \frac{\left(1 + K_{\mathrm{P\text{-}S}}\right)\left(k_0^{\mathbf{X}} + k_0^{\mathbf{X}\text{-S}}K_{\mathbf{X}\text{-S}}\right) + \left(k_0^{\mathbf{X}\text{-P}} + k_{\mathrm{q}}\right)K_{\mathbf{X}\text{-P}}[P_{\mathrm{o}}]}{\left(1 + K_{\mathrm{P\text{-}S}}\right)\left(1 + K_{\mathbf{X}\text{-S}}\right) + K_{\mathbf{X}\text{-P}}[\mathrm{P_o}]} \tag{S1.20}$$

It is convenient to combine $K_{\mathrm{P\text{-}S}}$, $K_{\mathbf{X}\text{-S}}$, and $K_{\mathbf{X}\text{-P}}$ by introducing an apparent solvent-specific H-bonding equilibrium constant between $\mathbf{X}^*$ and phenol

$$K_{\mathbf{X}\text{-P}}^{\mathrm{app}} = \frac{K_{\mathbf{X}\text{-P}}}{(1 + K_{\mathrm{P\text{-}S}})(1 + K_{\mathbf{X}\text{-S}})} \tag{S1.21}$$

which simplifies eq. S1.20 to

$$k_{\mathrm{obs}} = \frac{1}{\tau_{\mathrm{obs}}} = \frac{k_0^{\mathbf{X}} + k_0^{\mathbf{X}\text{-S}}K_{\mathbf{X}\text{-S}}}{\left(1 + K_{\mathbf{X}\text{-S}}\right)\left(1 + K_{\mathbf{X}\text{-P}}^{\mathrm{app}}[\mathrm{P_o}]\right)} + \frac{\left(k_0^{\mathbf{X}\text{-P}} + k_{\mathrm{q}}\right)K_{\mathbf{X}\text{-P}}^{\mathrm{app}}[P_{\mathrm{o}}]}{1 + K_{\mathbf{X}\text{-P}}^{\mathrm{app}}[\mathrm{P_o}]} \tag{S1.22}$$

With no added phenol ($[P_{\mathrm{o}}] = 0$), the solvent-specific decay rate constant, k_0, and lifetime, τ_0, are

$$k_0 = \frac{1}{\tau_0} = \frac{k_0^{\mathbf{X}} + k_0^{\mathbf{X}\text{-S}}K_{\mathbf{X}\text{-S}}}{1 + K_{\mathbf{X}\text{-S}}} = \frac{\tau_0^{\mathbf{X}}K_{\mathbf{X}\text{-S}} + \tau_0^{\mathbf{X}\text{-S}}}{\tau_0^{\mathbf{X}}\tau_0^{\mathbf{X}\text{-S}}\left(1 + K_{\mathbf{X}\text{-S}}\right)} \tag{S1.23}$$

so that the excited state decay rate constant observed without a quencher is a weighted average of the decay rates of the solvent-bound and free $\mathbf{X}^*$. As it should be expected, if the H-bonding to solvent does not occur ($K_{\mathbf{X}\text{-S}} = 0$) or does not alter the non-radiative and emissive decay rates ($k_0^{\mathbf{X}} = k_0^{\mathbf{X}\text{-S}}$), we simply have $k_0 = k_0^{\mathbf{X}}$.

The Stern-Volmer dependence that follows from eq. S1.22 and S1.23 is

$$\frac{k_{\text{obs}}}{k_0} = \frac{\tau_0}{\tau_{\text{obs}}} = 1 + \frac{\left(k_0^{\mathbf{X}\text{-P}} + k_{\text{q}} - k_0\right) K_{\mathbf{X}\text{-P}}^{\text{app}}[P_{\text{o}}]}{k_0\left(1 + K_{\mathbf{X}\text{-P}}^{\text{app}}[\text{P}_{\text{o}}]\right)} = 1 + \frac{\tau_{\text{o}}\left(k_{\text{q}} + 1/\tau_{\text{o}}^{\mathbf{X}\text{-P}} - 1/\tau_{\text{o}}\right) K_{\mathbf{X}\text{-P}}^{\text{app}}[\text{P}_{\text{o}}]}{1 + K_{\mathbf{X}\text{-P}}^{\text{app}}[\text{P}_{\text{o}}]} = 1 + \frac{\tau_{\text{o}} k_{\text{q}}^{\text{app}} K_{\mathbf{X}\text{-P}}^{\text{app}}[\text{P}_{\text{o}}]}{1 + K_{\mathbf{X}\text{-P}}^{\text{app}}[\text{P}_{\text{o}}]}$$

(S1.24)

where the apparent quenching rate constant is $k_{\text{q}}^{\text{app}} = k_0^{\mathbf{X}\text{-P}} + k_{\text{q}} - k_0 = k_{\text{q}} + 1/\tau_{\text{o}}^{\mathbf{X}\text{-P}} - 1/\tau_{\text{o}}$.

The observation of lifetime decrease upon addition of a quencher capable of hydrogen bonding means only that $k_0^{\mathbf{X}\text{-P}} + k_{\text{q}} > k_0$, but does not allow separate determination of k_{q} and $k_0^{\mathbf{X}\text{-P}}$ from the kinetic measurements. Only if $k_{\text{q}} \gg k_0^{\mathbf{X}\text{-P}} - k_0$, which is equivalent to suggesting that the H-bonding between $\mathbf{X}^*$ and phenol in $\mathbf{XP}^*$ does not dramatically accelerate the non-radiative and emissive deactivations, the determination of k_{q} becomes possible, as $k_{\text{q}}^{\text{app}} \approx k_{\text{q}}$. This suggestion is, of course, reasonable considering the relative weakness of the hydrogen bonding interactions. Although never discussed or even mentioned, the $k_{\text{q}} \gg k_0^{\mathbf{X}\text{-P}} - k_0$ assumption is implicit in all previous studies that postulated the hydrogen bonding between an excited metallocomplex and a quencher.[1-9]

It is obvious from eq. S1.24 that, if $K_{\mathbf{X}\text{-P}}^{\text{app}}[\text{P}_{\text{o}}] \ll 1$ in the entire measurement range, the Stern-Volmer plot will be approximately linear

$$\frac{k_{\text{obs}}}{k_0} = \frac{\tau_0}{\tau_{\text{obs}}} \approx 1 + \tau_{\text{o}} k_{\text{q}}^{\text{app}} K_{\mathbf{X}\text{-P}}^{\text{app}}[\text{P}_{\text{o}}] = 1 + \tau_{\text{o}} k_{\text{q}}^{\text{obs}}[\text{P}_{\text{o}}] \qquad \text{(S1.25)}$$

and the measurement of k_{obs} vs $[\text{P}_{\text{o}}]$ and k_0 can only yield a product of $k_{\text{q}}^{\text{app}}$ and $K_{\mathbf{X}\text{-P}}^{\text{app}}$; that is,

$$k_{\text{q}}^{\text{obs}} = k_{\text{q}}^{\text{app}} K_{\mathbf{X}\text{-P}}^{\text{app}} \qquad \text{(S1.26)}$$

Only with the data in the $K_{\mathbf{X}\text{-P}}^{\text{app}}[\text{P}_{\text{o}}] \gg 1$ range, when the Stern-Volmer plot approaches a plateau, can one separately determine $k_{\text{q}}^{\text{app}}$ and $K_{\mathbf{X}\text{-P}}^{\text{app}}$.

Case II. Steady-state emission

In the conventional steady state emission measurements the rate of excitation, R, is equal to the overall rate of excited state decay; that is,

$$R = k_0^{\mathbf{X}}[\mathbf{X}^*] + k_0^{\mathbf{X}\text{-S}}[\mathbf{X}\text{S}^*] + \left(k_0^{\mathbf{X}\text{-P}} + k_{\text{q}}\right)[\mathbf{X}\text{P}^*] = k_{\text{obs}}[\mathbf{X}_{\text{T}}^*] \qquad \text{(S1.27)}$$

where all concentrations $\mathbf{X}^*$, $\mathbf{X}\text{S}^*$, $\mathbf{X}\text{P}^*$, and $\mathbf{X}_{\text{T}}^*$ are in their steady states, and k_{obs} is given by eq. S1.22. We thus have $[\mathbf{X}_{\text{T}}^*] = R/k_{\text{obs}}$, and using eq. S1.13-S1.15, and S1.21 obtain

$$[\mathbf{X}^*] = \frac{R}{k_{\mathrm{obs}}\left(1 + K_{\mathbf{X}\text{-S}}\right)\left(1 + K_{\mathbf{X}\text{-P}}^{\mathrm{app}}[\mathrm{P_o}]\right)} \tag{S1.28}$$

$$[\mathbf{X}\mathrm{S}^*] = \frac{RK_{\mathbf{X}\text{-S}}}{k_{\mathrm{obs}}\left(1 + K_{\mathbf{X}\text{-S}}\right)\left(1 + K_{\mathbf{X}\text{-P}}^{\mathrm{app}}[\mathrm{P_o}]\right)} \tag{S1.29}$$

$$[\mathbf{X}\mathrm{P}^*] = \frac{RK_{\mathbf{X}\text{-P}}^{\mathrm{app}}[\mathrm{P_o}]}{k_{\mathrm{obs}}\left(1 + K_{\mathbf{X}\text{-P}}^{\mathrm{app}}[\mathrm{P_o}]\right)} \tag{S1.30}$$

The observed steady-state emission intensity at a given wavelength in the presence of a phenol quencher is

$$I_{\mathrm{obs}} = k'_{\mathrm{em}}[\mathbf{X}^*] + f''k''_{\mathrm{em}}[\mathbf{X}\mathrm{S}^*] + f''k'''_{\mathrm{em}}[\mathbf{X}\mathrm{P}^*] \tag{S1.31}$$

where f'' and f''' are the normalizing coefficients that account for the possible changes of the emission spectra of $\mathbf{X}\mathrm{S}^*$ and $\mathbf{X}\mathrm{P}^*$ compared to $\mathbf{X}^*$. Substituting here eq. S1.28-S1.30, we obtain

$$I_{\mathrm{obs}} = \frac{R}{k_{\mathrm{obs}}} \times \frac{k'_{\mathrm{em}} + f''k''_{\mathrm{em}}K_{\mathbf{X}\text{-S}} + f''k'''_{\mathrm{em}}\left(1 + K_{\mathbf{X}\text{-S}}\right)K_{\mathbf{X}\text{-P}}^{\mathrm{app}}[\mathrm{P_o}]}{\left(1 + K_{\mathbf{X}\text{-S}}\right)\left(1 + K_{\mathbf{X}\text{-P}}^{\mathrm{app}}[\mathrm{P_o}]\right)} \tag{S1.32}$$

The emission intensity in the absence of phenol ($[\mathrm{P_o}] = 0$) is

$$I_0 = \frac{R}{k_0} \times \frac{k'_{\mathrm{em}} + f''k''_{\mathrm{em}}K_{\mathbf{X}\text{-S}}}{1 + K_{\mathbf{X}\text{-S}}} \tag{S1.33}$$

The second factor on the right-hand side of this equation, $\frac{k'_{\mathrm{em}} + f''k''_{\mathrm{em}}K_{\mathbf{X}\text{-S}}}{1 + K_{\mathbf{X}\text{-S}}}$, has the same form as in eq. S1.23 and, similarly, can be considered a weighted average of the contributions to the emission from the solvent-bound and free $\mathbf{X}^*$.

From eq. S1.32 and S1.33, the Stern-Volmer dependence is

$$\frac{I_0}{I_{\mathrm{obs}}} = \frac{k_{\mathrm{obs}}}{k_0} \times \frac{\left(k'_{\mathrm{em}} + f''k''_{\mathrm{em}}K_{\mathbf{X}\text{-S}}\right)\left(1 + K_{\mathbf{X}\text{-P}}^{\mathrm{app}}[\mathrm{P_o}]\right)}{k'_{\mathrm{em}} + f''k''_{\mathrm{em}}K_{\mathbf{X}\text{-S}} + f'''k'''_{\mathrm{em}}\left(1 + K_{\mathbf{X}\text{-S}}\right)K_{\mathbf{X}\text{-P}}^{\mathrm{app}}[\mathrm{P_o}]} \tag{S1.34}$$

This equation shows that it is generally possible to obtain somewhat different dependencies of I_0/I_{obs} and k_{obs}/k_0 vs $[\mathrm{P_o}]$. It is however easy to see that, if the H-bonding interaction in $\mathbf{X}\mathrm{P}^*$ does not appreciably alter its emission spectrum from that observed in the absence of phenol (that is, if $f''k'''_{\mathrm{em}} = \frac{k'_{\mathrm{em}} + f''k''_{\mathrm{em}}K_{\mathbf{X}\text{-S}}}{1 + K_{\mathbf{X}\text{-S}}}$), the factor containing all k_{em} terms in eq. S1.34 is equal to unity, and the Stern-Volmer dependencies for I_{obs} and k_{obs} become exactly identical; that is,

$$\frac{I_0}{I_{\mathrm{obs}}} = \frac{k_{\mathrm{obs}}}{k_0} = 1 + \frac{\left(k_0^{\mathbf{X}\text{-P}} + k_{\mathrm{q}} - k_0\right)K_{\mathbf{X}\text{-P}}^{\mathrm{app}}[P_{\mathrm{o}}]}{k_0\left(1 + K_{\mathbf{X}\text{-P}}^{\mathrm{app}}[\mathrm{P_o}]\right)} = 1 + \frac{\tau_{\mathrm{o}}\left(k_{\mathrm{q}} + 1/\tau_{\mathrm{o}}^{\mathbf{X}\text{-P}} - 1/\tau_{\mathrm{o}}\right)K_{\mathbf{X}\text{-P}}^{\mathrm{app}}[P_{\mathrm{o}}]}{1 + K_{\mathbf{X}\text{-P}}^{\mathrm{app}}[\mathrm{P_o}]} = 1 + \frac{\tau_0 k_{\mathrm{q}}^{\mathrm{app}}K_{\mathbf{X}\text{-P}}^{\mathrm{app}}[P_{\mathrm{o}}]}{1 + K_{\mathbf{X}\text{-P}}^{\mathrm{app}}[\mathrm{P_o}]} \tag{S1.35}$$

Obviously, all restrictions on information about k_q and $K_{\mathbf{X}\text{-P}}^{app}$ that can be obtained from kinetic measurements discussed under eq. S1.24 fully apply to the steady state emission measurements as well.

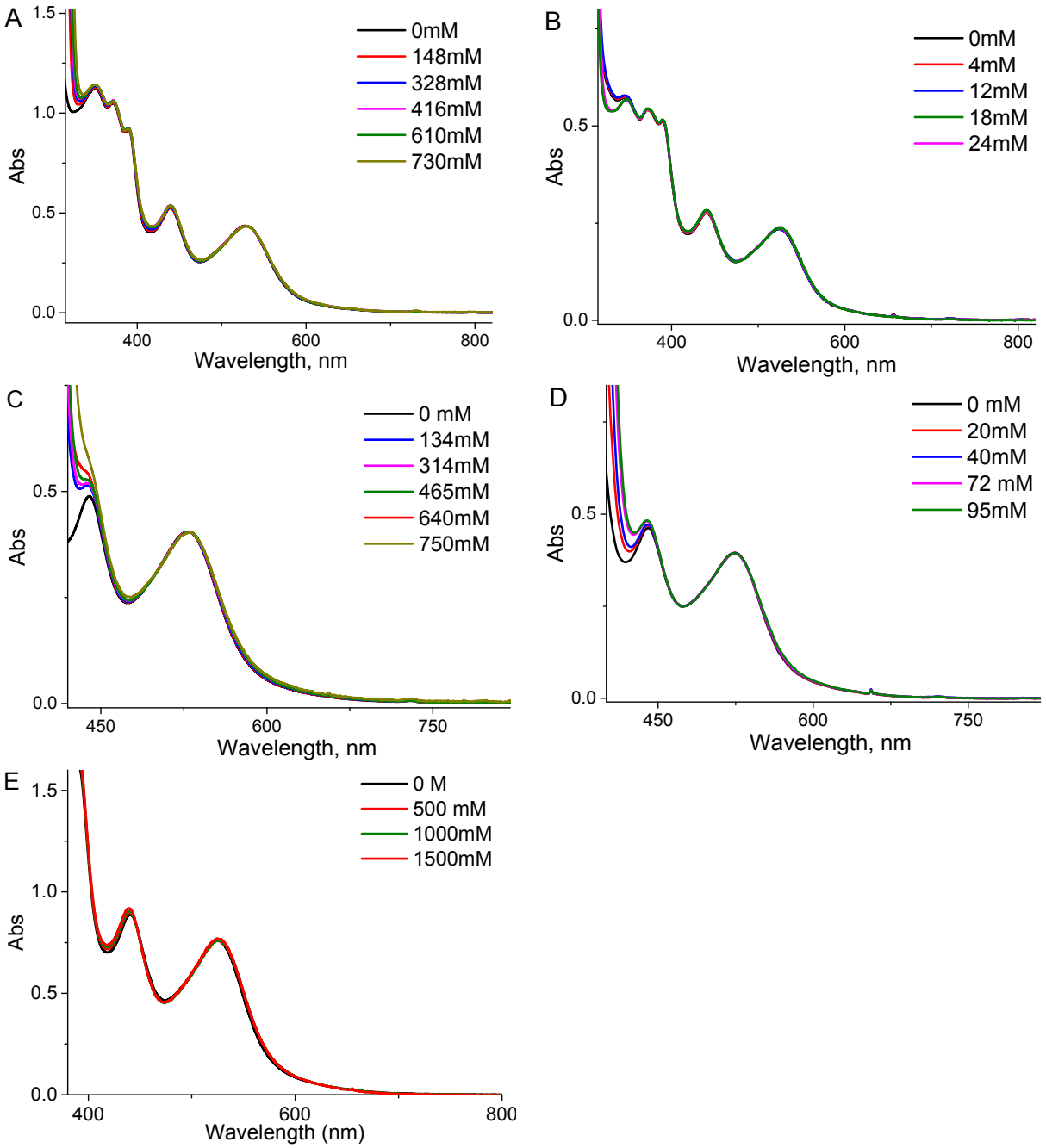

Figure S1. Absorption spectra of **1** (Scheme 1, main text) in the presence of phenols or trifluoroethanol in various concentrations. A: *p*-methoxyphenol in MeCN. B: *p*-methoxyphenol in CH_2Cl_2. C: *p*-nitrophenol in MeCN. D: *p*-nitrophenol in CH_2Cl_2. E: trifluoroethanol in CH_2Cl_2. Upon phenol or alcohol addition, these spectra exhibit no systematic variation of the 530 nm maximum of **1** that could be interpreted as the **1**-phenol/alcohol H-bonding. The apparent changes at shorter wavelengths (spectra A-D) are attributable to the additive contribution from phenol's absorption.

Section S2

Comparison with Previous Studies

In their investigation of EPT from a phenol-like donor (hydroquinone) to a $Ru(bpy)_2(bpz)^{2+}$ complex (bpy = 2,2′-bipyridine, bpz = 2,2′-bipyrazine; complex **2**) in a mixed H_2O/MeCN solvent, Meyer and co-workers reported a Stern-Volmer dependence for the transient emission decay rate constants that remained linear in the entire hydroquinone concentration range up to ~1.1 M, from which they determined the $k_q K_{\mathbf{2}\text{-P}}$ product to be 4.8×10^7 M^{-1} s^{-1}.[1] Remarkably, they were also able to independently determine the **2(T)**-hydroquinone H-bonding constant ($K_{\mathbf{2}\text{-P}}$) from the steady-state emission quenching measurements in the same hydroquinone concentration range. To this end, they derived the following equation that we present in its normalized form

$$\frac{1}{\Delta I_{\text{norm}}} = \frac{1}{1-C} + \frac{1}{(1-C)K_{\mathbf{2}\text{-P}}} \times \frac{1}{[\text{P}_\text{o}]} \qquad \text{(S2.1)}$$

Here, C is a dimensionless parameter whose magnitude is independent of the quencher concentration and ΔI_{norm} is the normalized emission decrease due to quenching; that is, $\Delta I_{\text{norm}} = (I_0 - I_{\text{obs}})/I_0$. By plotting $1/\Delta I_{\text{norm}}$ vs $1/[\text{P}_\text{o}]$, Meyer and co-workers obtained a straight line that gave $K_{\mathbf{2}\text{-P}}$; that is,

$$\frac{Intercept}{Slope} = K_{\mathbf{2}\text{-P}} \qquad \text{(S2.2)}$$

This independent determination of $K_{\mathbf{2}\text{-P}} \approx 11$ M^{-1} allowed them to disentangle the $k_q K_{\mathbf{2}\text{-P}}$ product in the Stern-Volmer dependence and obtain $k_q = 4.5\times10^6$ s^{-1}. We will now show that the determination of $K_{\mathbf{2}\text{-P}}$ and, through that, separation of k_q from $K_{\mathbf{2}\text{-P}}$ are impossible from the steady-state emission or transient emission and absorption data alone if a linear Stern-Volmer dependence is observed for any one I_{obs}, τ_{obs}, or k_{obs}.

Indeed, following Meyer and co-workers and neglecting both **2(T)**-solvent and hydroquinone-solvent H-bonding interactions, which is equivalent to setting $K_{\mathbf{2}\text{-P}} = K_{\text{P-S}} = 0$ in our eq. S1.21 (SI Section S1), we obtain $K_{\mathbf{2}\text{-P}}^{\text{app}} = K_{\mathbf{2}\text{-P}}$ and the Stern-Volmer equations for both I_{obs} and τ_{obs} (see eq. S1.24)

$$\frac{k_{\text{obs}}}{k_0} = \frac{\tau_0}{\tau_{\text{obs}}} = \frac{I_0}{I_{\text{obs}}} = 1 + \tau_0 k_q \frac{K_{\mathbf{2}\text{-P}}[\text{P}_\text{o}]}{1+K_{\mathbf{2}\text{-P}}[\text{P}_\text{o}]} \qquad \text{(S2.3)}$$

It is clear from this equation that at $K_{\mathbf{2}\text{-P}} \approx 11\ \text{M}^{-1}$ the Stern-Volmer dependence cannot remain close to linear beyond ~0.1 M hydroquinone concentration (Figure S2).

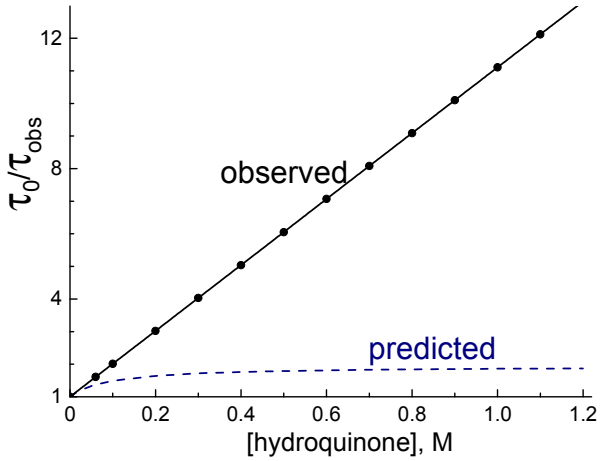

Figure S2. Solid line: time-resolved measurements by Meyer and co-workers[1] redrawn as a lifetime Stern-Volmer dependence for the reaction between **2(T)** and hydroquinone. Dashed line: Stern-Volmer dependence predicted by eq. S2.3 with $\tau_0 = 2.08\times10^{-7}$ s, $K_{\mathbf{2}\text{-P}}$=10.8 M^{-1}, and $k_\text{q} = 4.5\times10^{6}\ \text{s}^{-1}$.

In fact, a linear Stern-Volmer dependence up to 1 M concentration means that $K_{\mathbf{2}\text{-P}} \ll 1\ \text{M}^{-1}$, and eq. S2.3 can be approximated by

$$\frac{I_0}{I_{\text{obs}}} = \frac{\tau_0}{\tau_{\text{obs}}} \approx 1 + \tau_0 k_\text{q} K_{\mathbf{2}\text{-P}}[\text{P}_\text{o}] \qquad \text{(S2.4)}$$

It is also clear that the steady state measurements yield exactly the same information as the time-resolved measurements and that k_q and $K_{\mathbf{2}\text{-P}}$ cannot be individually determined from such data. Indeed, eq. S2.4 is readily transformed into the double reciprocal form of S2.1 used by Meyer and co-workers; that is,

$$\frac{1}{\Delta I_{\text{norm}}} = 1 + \frac{1}{\tau_0 k_\text{q} K_{\mathbf{2}\text{-P}}} \times \frac{1}{[\text{P}_\text{o}]} \qquad \text{(S2.5)}$$

so that the intercept/slope ratio for the $1/\Delta I_{\text{norm}}$ vs $1/[\text{P}_\text{o}]$ plot is

$$\frac{Intercept}{Slope} = \tau_0 k_\text{q} K_{\mathbf{2}\text{-P}} \qquad \text{(S2.6)}$$

Comparing eq. S2.4 and S2.5, we observe that the slopes of I_0/I_{obs} vs $[\text{P}_\text{o}]$ and $1/\Delta I_{\text{norm}}$ vs $1/[\text{P}_\text{o}]$ plots should be reciprocals of each other. Naturally, this is true for Meyer and co-

workers' data within their experimental uncertainty. From their k_{obs} vs [P_o] dependence, the Stern-Volmer constant is $\tau_0 k_q K_{\mathbf{2}\text{-P}} \approx 10$ M^{-1}, and their $1/\Delta I_{norm}$ vs $1/[P_o]$ slope is ~0.1 M. We maintain that the derivations of Meyer and co-workers and their eq. S2.1 and S2.2 are incorrect. The principal mistake in their derivations is the implicit erroneous assumption that the total steady-state concentration of the excited state is independent of the quencher concentration. Specifically, using our notations defined in SI Section S1 and combining their equations S3 and S4 (as in ref. 1 on page 3 of SI), we obtain for the steady state emission intensity

$$I_{obs} = [\mathbf{X}_T^*] \frac{\lambda_{\mathbf{X}} + \lambda_{\mathbf{X}\text{-P}} K_{\mathbf{X}\text{-P}} [P_o]}{1 + K_{\mathbf{X}\text{-P}} [P_o]} \qquad \text{(S2.7)}$$

where $\lambda_{\mathbf{X}}$ and $\lambda_{\mathbf{X}\text{-P}}$ have been defined by Meyer and co-workers as "*proportionality constants similar to molar absorptivities in absorption spectroscopy*". In their derivations of eq. S2.1 from eq. S2.7, Meyer and co-workers have treated $[\mathbf{X}_T^*]$ as a quantity that is independent of [P_o], which is incorrect. In fact, as shown by our eq. S1.22 in SI Section S1, the value of $[\mathbf{X}_T^*]$ is equal to R/k_{obs} and depends on [P_o] through k_{obs} (eq. S1.27 in SI Section S1). The increase in [P_o] results in the increase of k_{obs}, which, in turn, decreases $[\mathbf{X}_T^*]$. Unfortunately, the erroneous method for analyzing the I_{obs} vs [P_o] dependencies suggested by Meyer and co-workers was uncritically adopted by several other research groups.

In their studies[2] of EPT from a number of *p*-substituted phenols to $Ru(bpz)_3^{2+}$ (complex **3**) in MeCN, Bronner and Wenger used eq. S2.1- S2.2 and obtained $K_{\mathbf{3}\text{-P}}$ values that monotonically decreased with the substituent electron-withdrawing strength from ~1500 M^{-1} for MeO-PhOH to ~5 M^{-1} for NC-PhOH, a counterintuitive result considering that the HB donating propensity of phenols increase in the same order. At the same time, the Stern-Volmer plots for both τ_{obs} and I_{obs} obtained in that study were linear for all phenols, which according to eq. S2.3 is impossible with the k_q and $K_{\mathbf{3}\text{-P}}$ values reported in that work. Bewildered by this inconsistency, we have reinvestigated the most extreme (in terms of large $K_{\mathbf{3}\text{-P}}$) case of MeO-PhOH.

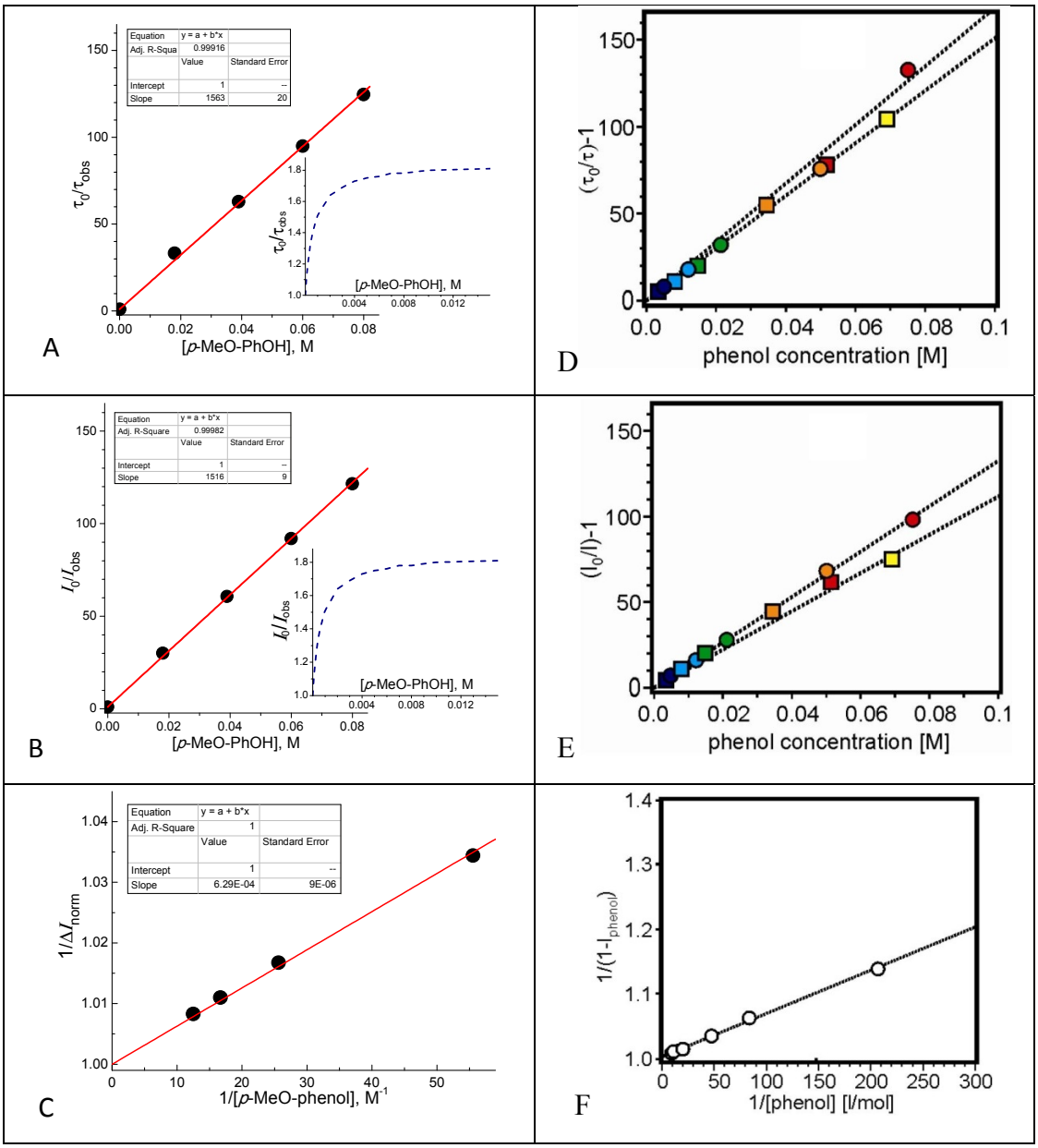

Figure S3. Side-by-side comparison of the quenching plots measured by us (A, B, and C) and reported by Bronner and Wenger[2] (D, E, and F). A and D: Stern-Volmer for lifetimes; B and E: Stern-Volmer for steady-state emission; C and F: steady-state emission data in reciprocal coordinates (as in eq. S2.5 in C, and S2.1 in F) for the reaction between **3(T)** and *p*-MeO-PhOH in MeCN. Squares in D and E represent the data for *p*-MeO-PhOD and should be ignored in this comparison. Notations ΔI_{norm} and $1 - I_{phenol}$ are equivalent. Insets in A and B show the Stern-Volmer dependencies predicted by eq. S2.3 with $\tau_0 = 4.6\times10^{-7}$ s, $K_{\mathbf{3}\text{-P}}$=1480 M^{-1}, and $k_q = 1.85\times10^6$ s^{-1} derived by Bronner and Wenger. Note a much smaller vertical inset scale. Panels D, E and F are reprinted with permission from *J. Phys. Chem. Lett.* **2012**, *3*, 70-74. Copyright 2012 American Chemical Society.

In Figure S3 we compare their data with our own measurements. In both cases, the Stern-Volmer plots correspond to eq. S2.4 and are numerically consistent between the measurements, and so are the steady-state emission data in the reciprocal coordinates. We maintain that the slope in panel C corresponds to eq. S2.5. Indeed, this slope yields $\tau_0 k_q K_{\mathbf{3}\text{-P}}$ = 1590 M^{-1}, which is in good agreement with the slopes in panels A and B. In contrast, Bronner and Wenger interpreted their essentially equivalent data in panel F in terms of eq. S2.1, concluded that $K_{\mathbf{3}\text{-P}}$ = 1478 M^{-1}, and used $\tau_0 = 4.6\times10^{-7}$ s to derive $k_q = 1.87\times10^6$ s^{-1}. As with the already discussed work of Meyer and co-workers, these set of parameters predicts rapidly saturating Stern-Volmer plots (insets in panels A and B) that are totally inconsistent with the measurements. Notably, the Stern-Volmer slopes in panels A and B (1560 and 1520 M^{-1}) are very close to the reciprocal of the slope in panel C ($1/6.3\times10^{-4}$ = 1590 M^{-1}) as predicted by eq. S2.4 and S2.5. In subsequent publications,[6,7] Wenger and co-workers used eq. S2.1 and S2.2 again, but, this time, they realized that the so-obtained $K_{\mathbf{3}\text{-P}}$ values are orders of magnitude too large to be compatible with linear Stern-Volmer plots that they observed. However, they refrained from inquiring into the origin of this problem and resorted to an equally untenable procedure involving the two-parameter fitting of the Stern-Volmer slopes, $\tau_0 k_q K_{\mathbf{3}\text{-P}}$. Obviously, this procedure can produce any number of arbitrary pairs of $K_{\mathbf{3}\text{-P}}$ and k_q.

Nocera and co-workers also treated their steady-state emission quenching data through eq. S2.1 and S2.2 to obtain binding constants between an MLCT-excited Re complex containing a ligand with a peripheral phenolic group (tyrosine) and bases (pyridine and imidazole) in CH_2Cl_2.[5] These artefactual constants were subsequently used to extract k_q for EPT reactions between the complex and the bound bases through fitting the k_{obs} vs [P_o]. Moreover, the k_{obs} vs [P_o] dependencies shown in their Figure S1[5] do not contain sufficient data for evaluating the plot curvatures and, therefore, k_q with an acceptable accuracy even if for fitting with the correct H-bonding constants.

Finally, we mention studies by Rajagopal and co-workers who employed eq. S2.1 and S2.2 for determining association constants between Ru and Os polyimine complexes and various redox reactive phenolic quenchers in water.[4,8] The consequences are the same, *i.e.*, erroneous binding constants and other reactivity parameters derived from them.

Recently, Hammarström and co-workers[9] criticized the use of $1/\Delta I_{\mathrm{norm}}$ vs $1/[\mathrm{P_o}]$ dependence for separating k_{q} and $K_{\mathbf{X}\text{-P}}$ as suggested by Meyer and co-workers and reported the Stern-Volmer plots for quenching an excited Re complex containing a head-on 4,4′-bipyridine ligand by phenols in MeCN that appear to show some downward deviation from linearity. However, the deviations are small (~10%) and the observed Stern-Volmer dependencies stop far short of saturation predicted by eq. S2.3. Due to these data shortcomings, the two-parameter fitting of these dependencies should yield only rough estimates (at the very best, within a factor of 2) for k_{q} and $K_{\mathbf{X}\text{-P}}$. Perhaps in recognition of this fact, Hammarström and co-workers resorted to setting $K_{\mathbf{X}\text{-P}}$ = 1 M^{-1} for all phenols employed, a questionable proposition considering a fairly broad variation of their HB acidity.

We conclude this section with considering a general case, without making any assumptions about magnitudes of $K_{\mathbf{X}\text{-P}}$, $K_{\mathrm{S}\text{-P}}$, and $K_{\mathbf{X}\text{-S}}$. From eq. S1.35 (SI Section S1) the steady-state emission intensity decrease upon quencher addition is

$$\Delta I_{\mathrm{norm}} = \frac{I_0 - I_{\mathrm{obs}}}{I_0} = \frac{\tau_0 k_{\mathrm{q}}^{\mathrm{app}} K_{\mathbf{X}\text{-P}}^{\mathrm{app}} [\mathrm{P_o}]}{1 + K_{\mathbf{X}\text{-P}}^{\mathrm{app}} [\mathrm{P_o}] + \tau_0 k_{\mathrm{q}}^{\mathrm{app}} K_{\mathbf{X}\text{-P}}^{\mathrm{app}} [\mathrm{P_o}]} \qquad \text{(S2.8)}$$

where $K_{\mathbf{X}\text{-P}}^{\mathrm{app}}$ and $k_{\mathrm{q}}^{\mathrm{app}}$ are defined by eq. S1.21 and S1.24, respectively.

Eq. S2.8 equation linearizes to

$$\frac{1}{\Delta I_{\mathrm{norm}}} = \frac{1 + \tau_0 k_{\mathrm{q}}^{\mathrm{app}}}{\tau_0 k_{\mathrm{q}}} + \frac{1}{\tau_0 k_{\mathrm{q}}^{\mathrm{app}} K_{\mathbf{X}\text{-P}}^{\mathrm{app}}} \times \frac{1}{[\mathrm{P_o}]} \qquad \text{(S2.9)}$$

so that the intercept/slope ratio for the $1/\Delta I_{\mathrm{norm}}$ vs $1/[\mathrm{P_o}]$ plot is

$$\frac{Intercept}{Slope} = \left(1 + \tau_0 k_{\mathrm{q}}^{\mathrm{app}}\right) K_{\mathbf{X}\text{-P}}^{\mathrm{app}} \qquad \text{(S2.10)}$$

It is now obvious that a $1/\Delta I_{\mathrm{norm}}$ vs $1/[\mathrm{P_o}]$ plot is always linear, irrespective of whether the corresponding Stern-Volmer plot is linear ($K_{\mathbf{X}\text{-P}}^{\mathrm{app}}[\mathrm{P_o}] \ll 1$ in the entire $[\mathrm{P_o}]$ range) or saturating ($K_{\mathbf{X}\text{-P}}^{\mathrm{app}}[\mathrm{P_o}] \gg 1$ at the high end of $[\mathrm{P_o}]$ range). However, a $1/\Delta I_{\mathrm{norm}}$ vs $1/[\mathrm{P_o}]$ plot is practically useless for separating $K_{\mathbf{X}\text{-P}}^{\mathrm{app}}$ and $k_{\mathrm{q}}^{\mathrm{app}}$ because we are generally not interested in cases for which chemical quenching does not efficiently competes with the excited state self-deactivation and $\tau_0 k_{\mathrm{q}}^{\mathrm{app}} \ll 1$. If $\tau_0 k_{\mathrm{q}}^{\mathrm{app}} \gg 1$, eq. S2.9 and S2.10 become equivalent to the already-discussed eq. S2.5 and S2.6.

In their criticism of the prior works by Meyer and co-workers[1] and Bronner and Wenger,[2] Hammarström and co-workers maintain that the data exhibiting linearity in both $1/\Delta I_{\text{norm}}$ vs $1/[\text{P}_\text{o}]$ and Stern-Volmer coordinates in those studies "*can be explained by diffusional quenching*" and "*clearly suggest a simple diffusional quenching*".[9] While the former statement is correct, the latter statement is unnecessarily restrictive. In fact, diffusional quenching is not requisite for simultaneous linearity of the $1/\Delta I_{\text{norm}}$ vs $1/[\text{P}_\text{o}]$ and Stern-Volmer plots. Whether the quenching is diffusional or occurs through the intermediacy of a precursor complex due to H-bonding or any other interaction (*e.g.*, ion pairing), eq. S2.9 clearly shows that a $1/\Delta I_{\text{norm}}$ vs $1/[\text{P}_\text{o}]$ plot should be linear. Thus, according to eq. S2.9 and S1.35, the observation of linear plots for both $1/\Delta I_{\text{norm}}$ vs $1/[\text{P}_\text{o}]$ and k_{obs}/k_0 vs $[\text{P}_\text{o}]$ by Meyer and co-workers[1] and Bronner and Wenger[2] are actually consistent with the intermediacy of H-bonded precursor complex provided that $K_{\mathbf{X}\text{-P}}^{\text{app}}[\text{P}_\text{o}] \ll 1$ in the entire $[\text{P}_\text{o}]$ range.

Section S3

Flash Photolysis data for the 1-Trifluoroethanol and 1-MeOPhOH Systems

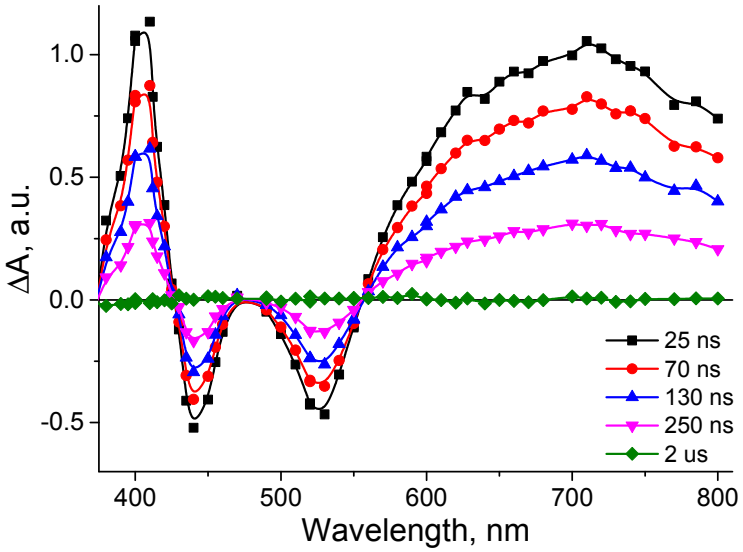

Figure S4. Transient absorption spectra recorded at the indicated times following a 532 nm laser flash photolysis of N_2-saturated acetonitrile solution of **1** containing 1 M of trifuoroethanol.

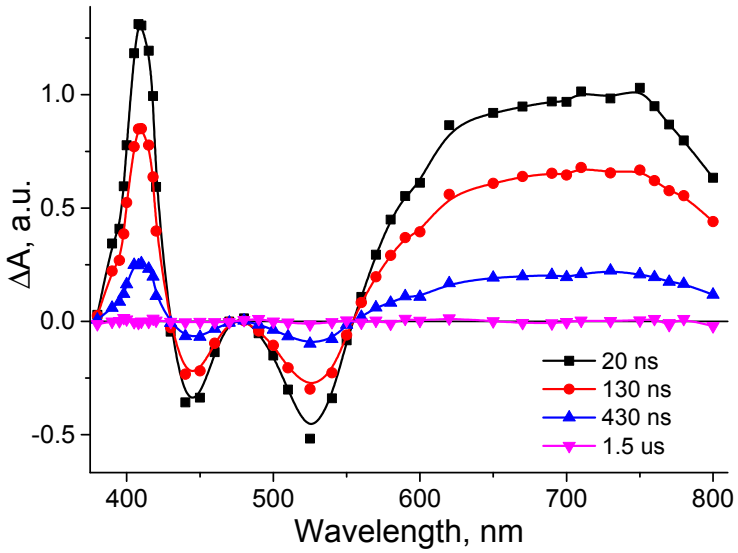

Figure S5. Transient absorption spectra recorded at the indicated times following a 532 nm laser flash photolysis of N_2-saturated dichloromethane solution of **1** containing 1 M of trifuoroethanol.

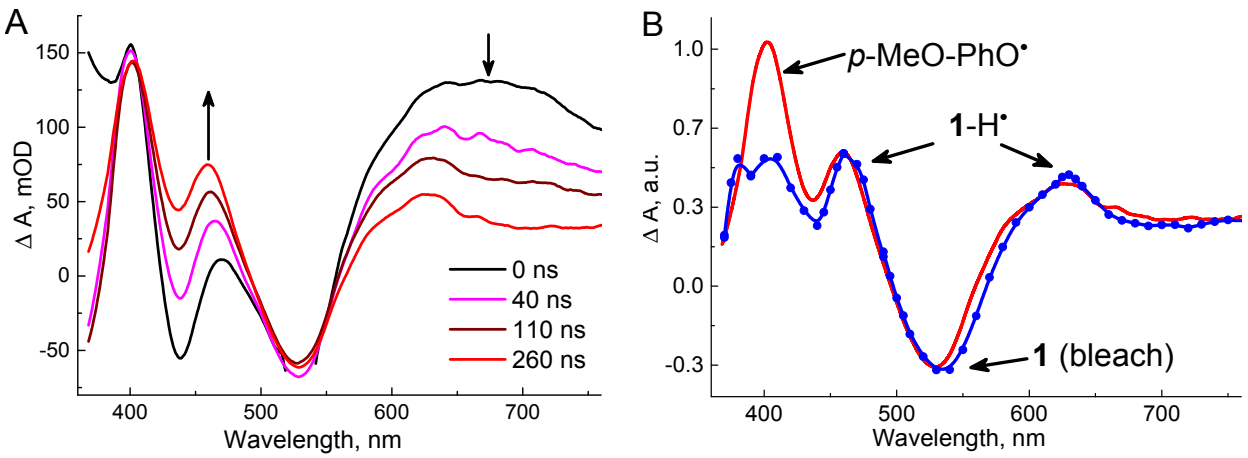

Figure S6. A: transient absorption spectra recorded at the indicated times following 532 nm laser flash photolysis of complex **1** in Ar-purged acetonitrile containing 200 mM of *p*-methoxy-phenol. The prompt spectrum at 0 ns is due to the **1(T)** absorption only; the spectrum is truncated around 532 nm due to detector saturation by scattered laser light. The final spectrum corresponds to the difference between absorptions by the nascent products from the quenching reactions and that of **1** in its ground state; this spectrum is taken after the quenching completion, but before any subsequent second-order reactions between the products could occur. B: overlay of the final spectrum at 260 ns from panel A (red solid line) and the spectrum of **1**-H$^{\bullet}$ previously measured[10] through pulse radiolysis (blue dotted line); the two spectra are normalized at the 530 nm bleaching minimum of **1** for comparison.

Section S4

Experimental Stern-Volmer Dependencies for Steady-State and Time-Resolved Emission Quenching of Complex 1 and 1i by *p*-Substituted Phenols

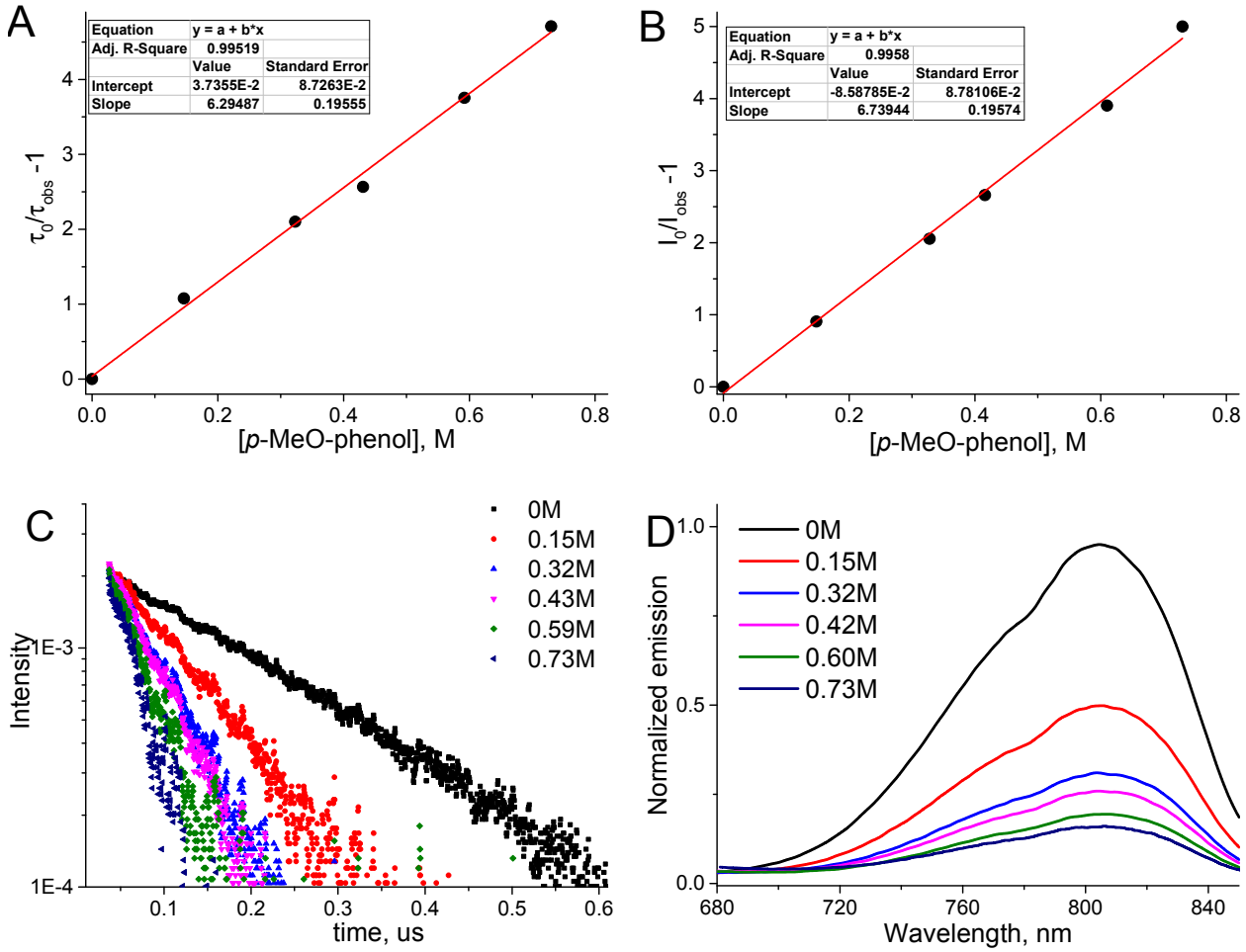

Figure S7. A: Stern-Volmer lifetime and B: steady-state emission quenching plots for the reaction between **1(T)** and *p*-methoxyphenol in MeCN. C: Representative kinetic and D: steady state emission data.

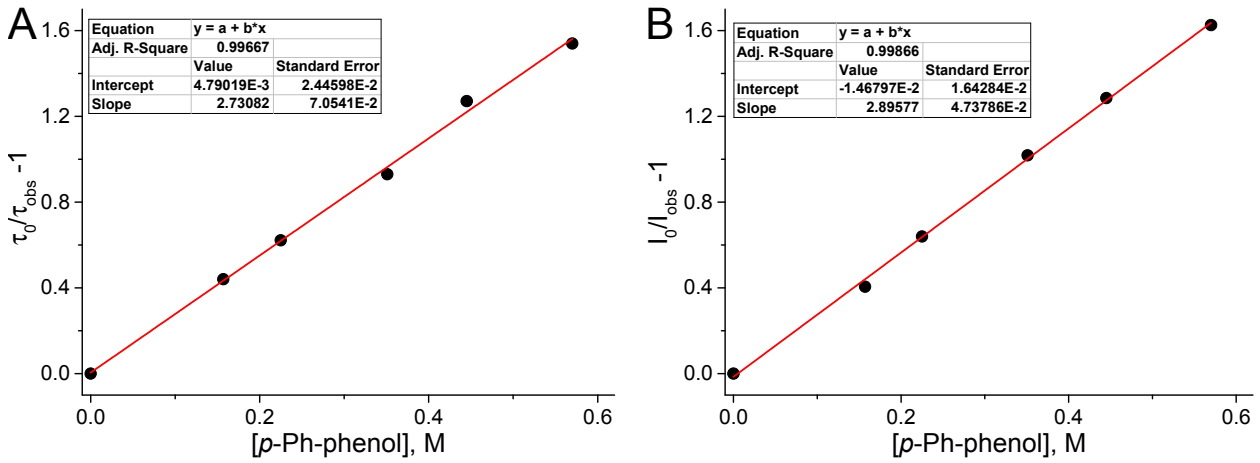

Figure S8. A: Stern-Volmer lifetime, and B: steady-state emission quenching plots for the reaction between **1(T)** and *p*-phenylphenol in MeCN. Note, that the maximum concentration of *p*-phenylphenol was limited by its solubility.

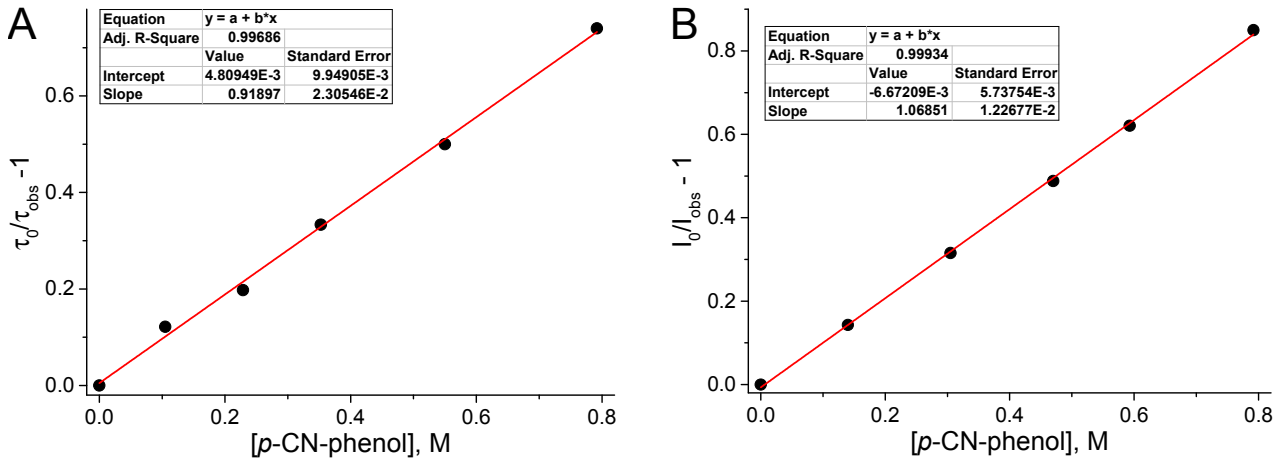

Figure S9. A: Stern-Volmer lifetime, and B: steady-state emission quenching plots for the reaction between **1(T)** and *p*-cyanophenol in MeCN.

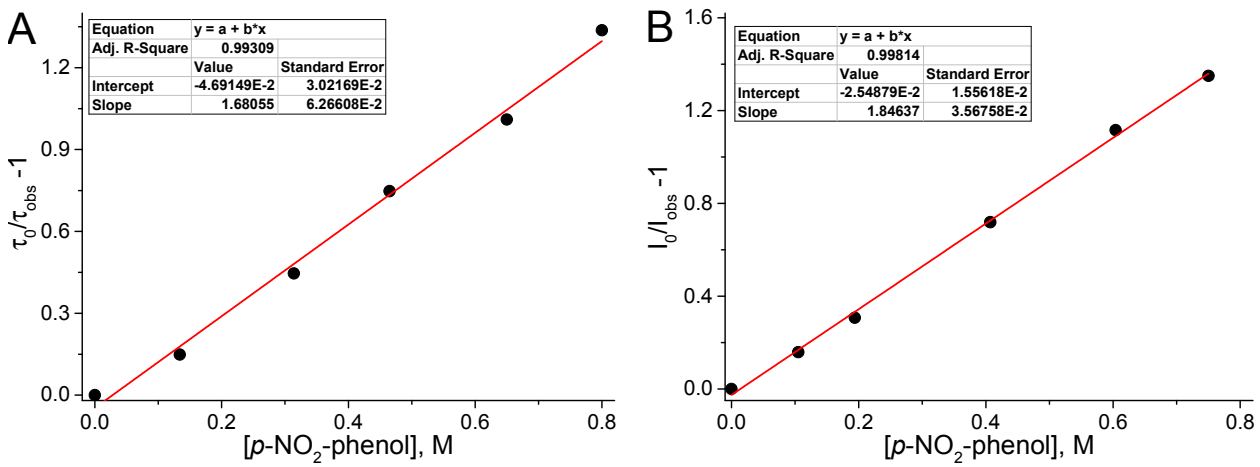

Figure S10. A: Stern-Volmer lifetime, and B: steady-state emission quenching plots for the reaction between **1(T)** and *p*-nitrophenol in MeCN.

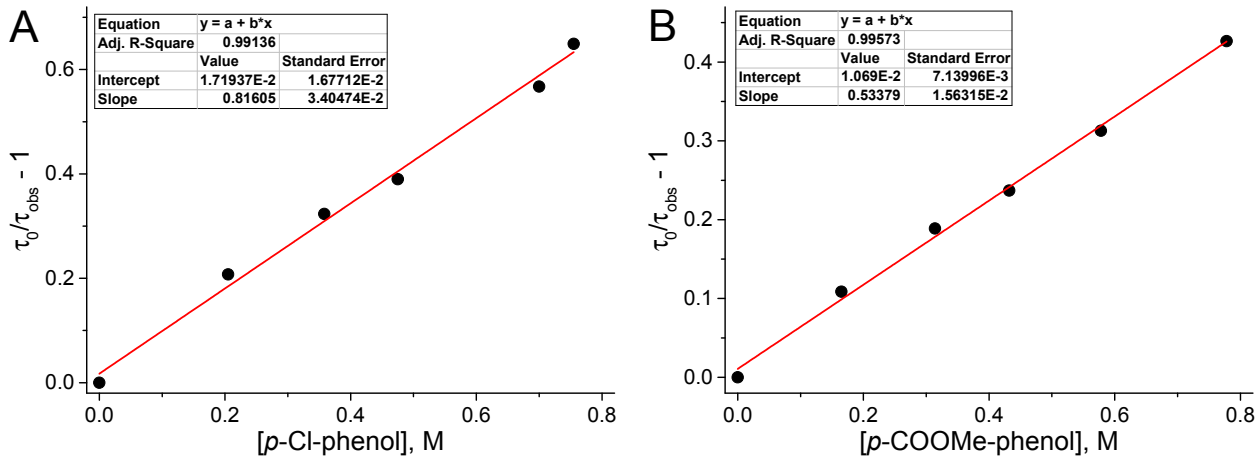

Figure S11. Stern-Volmer emission lifetime quenching plots for the reaction between **1(T)** and *p*-chlorophenol (A) and methyl 4-hydroxybenzoate (B) in MeCN.

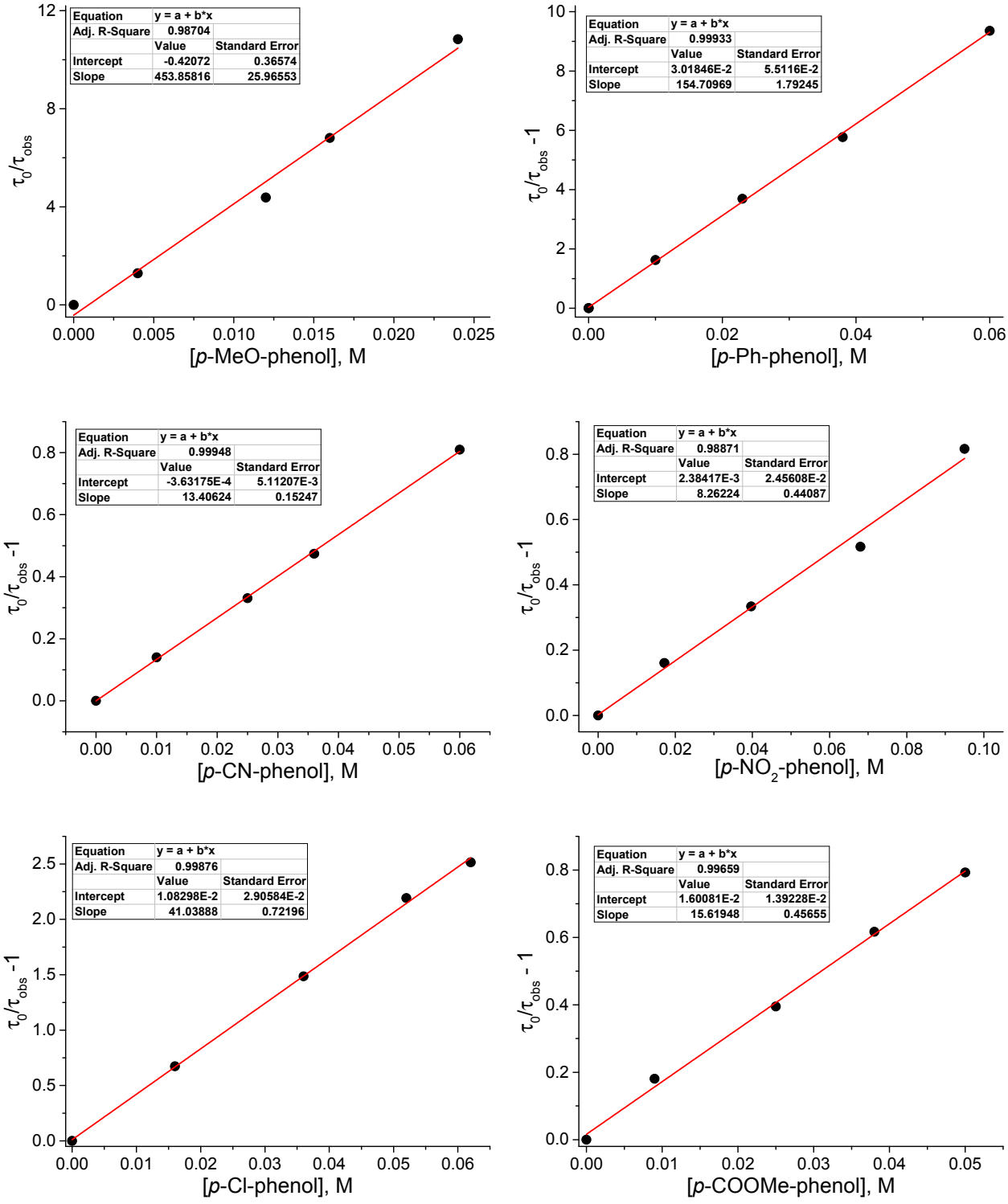

Figure S12. Stern-Volmer lifetime quenching plots for the reaction between **1(T)** and *p*-substituted phenols in CH_2Cl_2.

Table S1. Room temperature photophysical and redox properties of metal complexes **1** and **1i** in water, acetonitrile and dichloromethane

Solvent	λ_{max} (abs.)[a]	λ_{max} (emis.)[b]	τ_0(T)[b]	$E_{1/2}$ ($\mathbf{X}/\mathbf{X}^{\bullet-}$)[c]	E^0 ($\mathbf{X}$(T)/$\mathbf{X}^{\bullet-}$)
Complex **1**					
H_2O	536	814	30	–0.77[11]	1.17[d]
MeCN	528	804	190	–0.72[12]	0.60[e]
CH_2Cl_2	525	796	350	nd	nd
Complex **1i**					
H_2O	552	820	8	–0.75[13]	1.19[d]
MeCN	552	820	70	–0.75[12]	0.57[e]
CH_2Cl_2	549	814	136	nd	nd

[a]MLCT band, λ in nm, ± 2 nm; [b]Triplet emission, λ in nm, ±5 nm; τ_0 in ns, ± 5 ns; [c]E in V reported vs SCE; [d]E in V referenced to SHE; [e]E in V referenced to $Fc^{+/0}$ in MeCN. Aqueous pK_as: 1.7 (**1**); 0.2 (**1i**).[12]

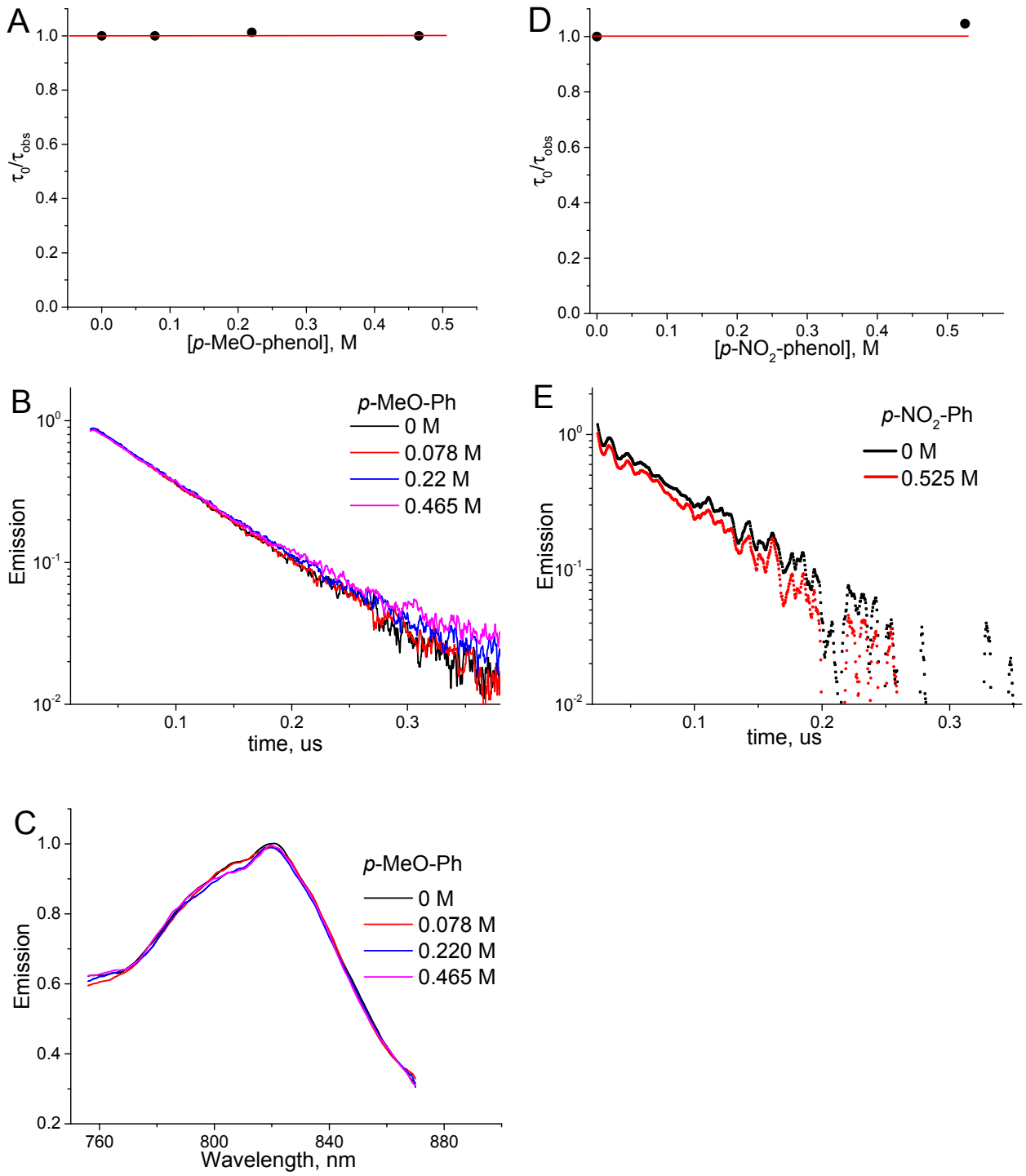

Figure S13. Quenching data for the reaction between **1i(T)** and *p*-methoxyphenol (A, B, C) and *p*-nitrophenol (D, E) in MeCN.

Section S5

Arrhenius and Eyring Plots from Time-Resolved Emission Measurements for Complex 1 in MeCN

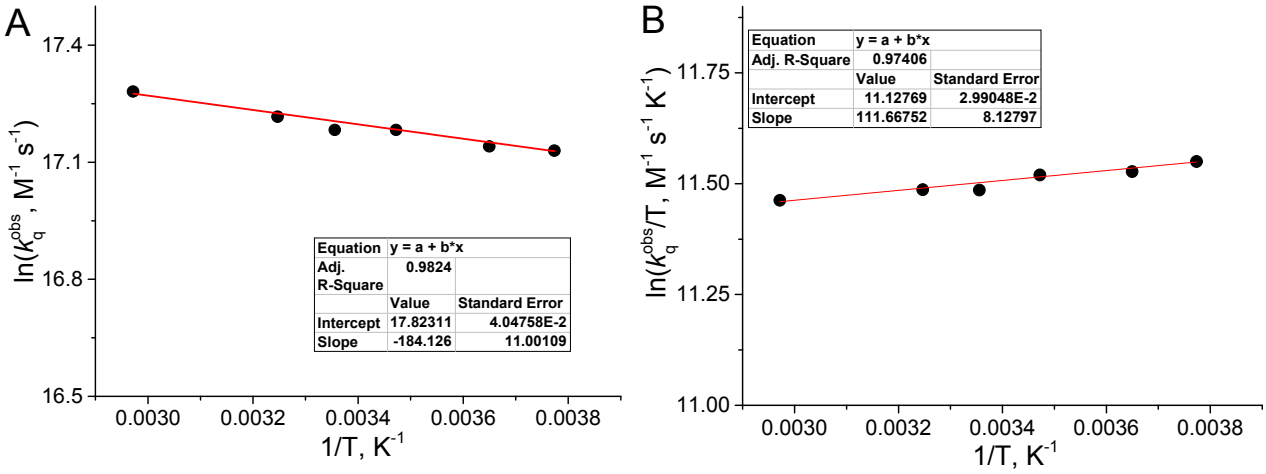

Figure S14. Arrhenius (A) and Eyring (B) plots for the reaction between **1(T)** and *p*-methoxyphenol in MeCN.

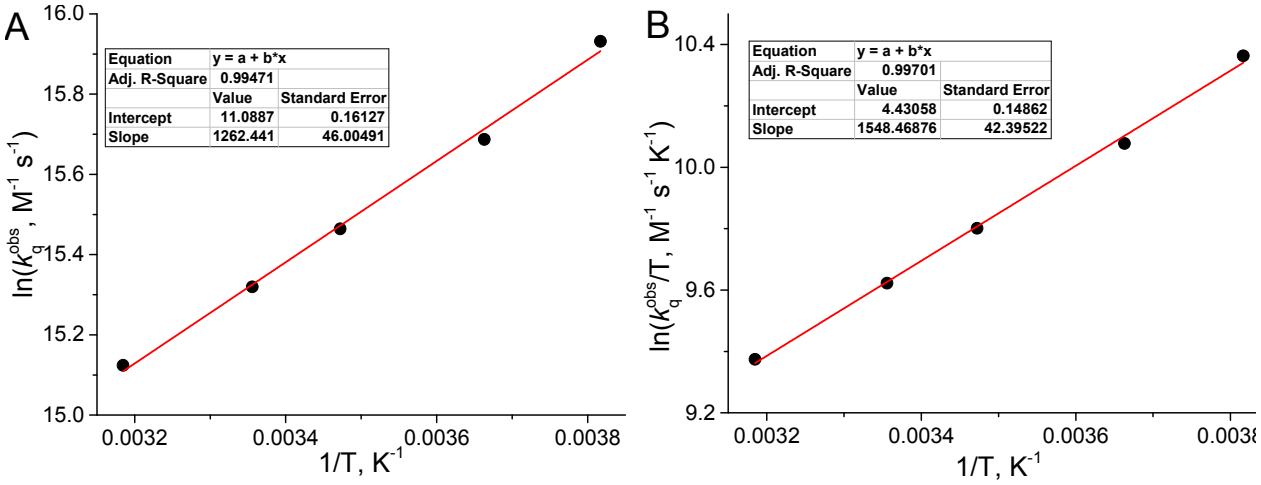

Figure S15. Arrhenius (A) and Eyring (B) plots for the reaction between **1(T)** and *p*-cyanophenol in MeCN.

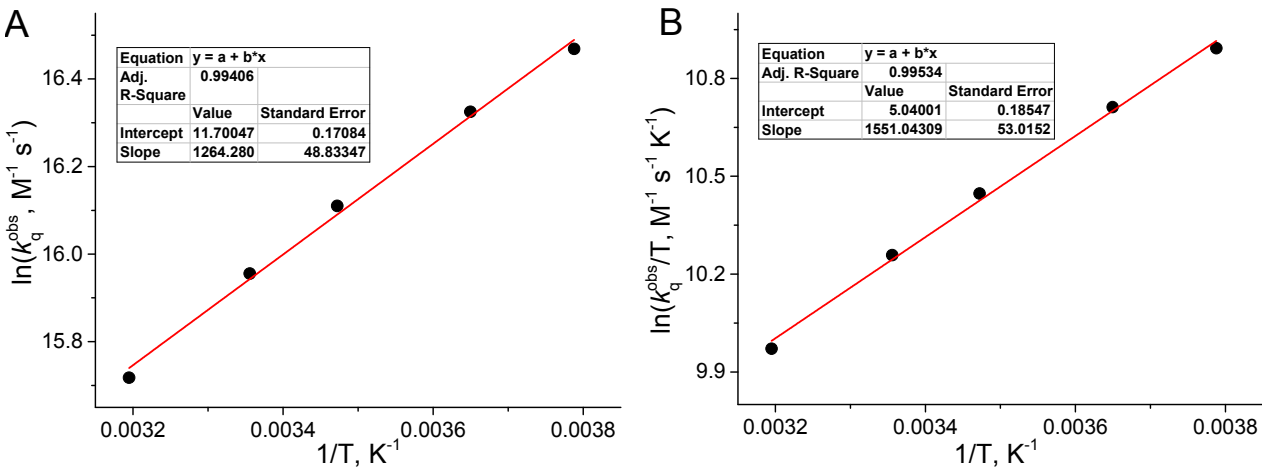

Figure S16. Arrhenius (A) and Eyring (B) plots for the reaction between **1(T)** and *p*-nitrophenol in MeCN.

Section S6

Activation Parameters and Hydrogen Bonding

Due to the high HB basicity and low HB acidity of MeCN ($K_{\text{P-S}} \gg 1$, and expected $K_{\mathbf{1}\text{-S}} \ll 1$), eq. 5 (main text) simplifies to $k_{\text{q}}^{\text{obs}} \approx k_{\text{q}}\, K_{\mathbf{1}\text{-P}}/K_{\text{P-S}}$, and the observed activation enthalpy is

$$\Delta H_{\text{obs}}^{\ddagger} \approx \Delta_{\text{q}}H^{\ddagger} + \Delta_{\mathbf{1}\text{-P}}H - \Delta_{\text{P-S}}H \qquad \text{(S6.1)}$$

where $\Delta_{\mathbf{1}\text{-P}}H$ and $\Delta_{\text{P-S}}H$ are the H-bonding enthalpies in **1**(**T**)-P and P-S, respectively, and $\Delta_{\text{q}}H^{\ddagger}$ is the activation enthalpy of the chemical quenching step within the **1(T)**-P precursor complex. The observed activation entropy obeys a similar equation

$$\Delta S_{\text{obs}}^{\ddagger} \approx \Delta_{\text{q}}S^{\ddagger} + \Delta_{\mathbf{1}\text{-P}}S - \Delta_{\text{P-S}}S \qquad \text{(S6.2)}$$

The value of $\Delta_{\text{P-S}}H$ can be estimated from the empirical correlation developed by Ingold and co-workers for the H-bonding enthalpy between the phenolic solutes and a neat solvent;[14] that is,

$$\Delta_{\text{P-S}}H = -20.56\alpha_2^{\text{H}}(\text{P})\beta_2^{\text{H}}(\text{S}) + 0.59, \text{ kcal/mol at 25 }^{\text{o}}\text{C} \qquad \text{(S6.3)}$$

The $\Delta_{\text{P-S}}H$ values obtained from this equation shown in Table 2 (main text) are substantially negative and, as expected, decrease with the phenol's HB acidity.

The negative apparent activation enthalpy is, we believe, best explained by the precursor complex formation, whose $\Delta_{\mathbf{1}\text{-P}}H$ term in eq. S6.1 is sufficiently negative to exceed the combined positive contributions to $\Delta H_{\text{app}}^{\ddagger}$ from the solvent-phenol H-bonding and activation enthalpy of the chemical quenching step. The computations indicate that the phenols' H-bonds to **1(T)** are stronger than to MeCN, which makes the $\Delta_{\mathbf{1}\text{-P}}H - \Delta_{\text{P-S}}H$ difference in eq. S6.1 about 4 kcal/mol negative for all MeOPhOH, NCPhOH, and O_2NPhOH. Taken at their face values, the computed $\Delta_{\mathbf{1}\text{-P}}H - \Delta_{\text{P-S}}H$ values would account for $\Delta H_{\text{obs}}^{\ddagger}$ provided that $\Delta_{\text{q}}H^{\ddagger}$ terms are sufficiently small and the quenching step by MeOPhOH is somewhat more strongly activated than by NCPhOH and O_2NPhOH. This difference is likely to arise from the change of quenching mechanism that will be discussed later in a future publication.

From eq. 3 (main text), which is

$$logK_{\text{P-S}} = 7.354\alpha_2^{\text{H}}(\text{P})\beta_2^{\text{H}}(\text{S}) + log[\text{S}] - 1.094 \qquad \text{(S6.4)}$$

the following expression can be obtained

$$\Delta_{\text{P-S}}G = -10.03\alpha_2^{\text{H}}(\text{P})\beta_2^{\text{H}}(\text{S}) - 1.364log[\text{S}] + 1.492, \text{ kcal/mol} \qquad \text{(S6.5)}$$

Combining eq. S6.3 and eq. S6.5 we obtain the H-bonding entropy at 25 $^{\text{o}}$C

$$\Delta_{\text{P-S}}S = -35.3\alpha_2^{\text{H}}(\text{P})\beta_2^{\text{H}}(\text{S}) + 4.6\,log[\text{S}] - 3.0,\ \text{cal/(mol K)} \qquad \text{(S6.6)}$$

As expected for an association process, the considerably negative $\Delta_{\text{P-S}}S$ values are estimated through this equation: −6 for MeOPhOH, −9 for NCPhOH, and −10 cal/(mol K) for O_2NPhOH (Table 2, main text).

The net entropy decrease upon H-bonding arises from the loss of phenol's translational and, partially, rotational degrees of freedom that are transformed into less entropy-contributing soft vibrations. Although this applies to both **1(T)** and MeCN HB acceptors, we should expect the $\Delta_{\mathbf{1}\text{-P}}S$ term in eq. S6.2 to be more negative than the $\Delta_{\text{S-P}}S$ term. Indeed, the computed stronger phenol binding to **1(T)** than to MeCN (negative $\Delta_{\mathbf{1}\text{-P}}H - \Delta_{\text{P-S}}H$) should result in greater restrictions on phenolic movement and in stiffening of the soft vibrational modes. This effect is implicit in the Abraham-Ingold model, whose eq. S6.3 and S6.6 predict a linear ΔS-ΔH correlation. If this model were applicable to the **1(T)**-phenol bonding, the result would have been

$$(\Delta_{\mathbf{1}\text{-P}}S - \Delta_{\text{P-S}}S) = 1.72(\Delta_{\mathbf{1}\text{-P}}H - \Delta_{\text{P-S}}H) - 4.6\,log[\text{S}] \approx -(12\text{-}13),\ \text{cal/(mol K)} \qquad \text{(S6.7)}$$

Because the Abraham-Ingold empirical model is trained on data sets that do not include contribution from the entropy-decreasing charge-dipole electrostatic interactions between the H-bonded species, which can be significant in the **1(T)**-phenol association due to substantial dipole moments of phenols, eq. S6.7 should be considered nothing more than a crude estimate. It is introduced here mainly to emphasize that the magnitude of the negative $(\Delta_{\mathbf{1}\text{-P}}S - \Delta_{\text{P-S}}S)$ term in eq. S6.2 is very likely insufficient to account for the very negative $\Delta S^{\ddagger}_{\text{obs}}$ values in Table 2 (main text), and the activation entropies for the quenching step must therefore be substantially negative, perhaps as much as −(10-20) cal/(mol K). We defer interpreting this assertion to a forthcoming publication.

Section S7

Computational Data at the M06/def2-TZVP Level of Theory

All molecular structures were fully optimized at the M06 level of density functional theory[15-17] with the SMD continuum solvation model[18] for MeCN and CH_2Cl_2 as solvents using the Stuttgart [8s7p6d2f | 6s5p3d2f] ECP28MWB contracted pseudopotential basis set[19] on Ru and the 6-31G(d) basis set on all other atoms.[20] Non-analytical integrals were evaluated using the integral=grid=ultrafine option as implemented in the Gaussian 09 software package.[21] The nature of all stationary points was verified by analytic computation of vibrational frequencies that were also used for the computation of zero-point vibrational energies and molecular partition functions. The latter were used in the computations of the 298 K thermal contributions to free energy employing the usual ideal-gas, rigid-rotator, harmonic oscillator approximation.[22] Free-energy contributions were added to single-point, SMD-solvated M06 electronic energies computed at the optimized geometries obtained with the initial basis with the def2-TZVPP basis set on Ru and the def2-TZVP basis set[23] on all other atoms to arrive at the final, composite free energies. A 1 M standard state was used for all species in solution. Thus, the free energy in solution is computed as the 1 atm gas-phase free energy, plus a 1.9 kcal/mol adjustment for the 1 atm to 1 M gas standard-state concentration change, plus the free energy of 1 M gas to 1 M solute transfer (solvation) computed from the SMD model.

For the performance evaluation of our computations in describing the thermochemistry of hydrogen bonding, we have chosen a widely-studied pyridine-phenol H-bonding as a benchmark case. The comparison of computed and experimental data presented in Table S2 shows that the computed free energy is about 2.5 kcal/mol too high. Although the computational enthalpy comes within 0.6 kcal/mol to the best experimental value, the computed entropy decrease is substantially (by ~10 cal/(mol K)) overestimated. A similar pattern is found when comparing computed thermochemistry with that evaluated from empirical correlations for H-bonding between phenols and MeCN in CCl_4 (Table S3). Again, the computations reproduce the enthalpy within 0.5 kcal/mol, but overestimate the entropy decrease by 7-11 cal/(mol K), which results in the free energy error of ~2 kcal/mol that is too large for the present purposes. The systematic overestimation of entropy decrease arises, we believe, from the computational difficulties in accounting for the very soft anharmonic vibrations associated with H-bonding. For that reason, we use the explicit hydrogen bonding computations only for the enthalpy evaluations in this

work. However, for exploring the trends in electron, proton, and electron-proton transfer reactions we do use the free energy computations and expect the computational errors to largely cancel out in ΔG^0 and, especially, in $\Delta\Delta G^0$ values.

Table S2. Comparison of experimental literature with computed in this work thermochemistry (in kcal/mol and cal/(mol K) at 298 K) for H-bonding between unsubstituted phenol and pyridine (pyr). All data are for the CCl_4 solvent ($\alpha_2^H = \beta_2^H = 0$), except where indicated otherwise. Also included are values obtained through the empirical correlations given by eq. S6.3 and S6.5 (with S = pyridine and $log[S] = 0$, which accounts for the pyridine solute standard state of 1 M in a given solvent). The values in red, reported by Arnett and co-workers (obtained from IR and calorimetric measurements)[24] are regarded as the most reliable and are used for benchmarking.

Source	$-\Delta_{HB}G$	$-\Delta_{HB}H$	$-\Delta_{HB}S$
Experiment (PhOH)	**2.3**[24] 2.2[25] 2.4[26] 1.9[27, a] 2.3[28] 2.4[29]	**7.0**[24] 9.0[25] 6.5[26] 6.5[27,30, a] 7.5[28] 7.0[29] 6.2[31]	**15.7**[24] 23[25] 14.0[26] 15.6[27, a] 17.4[28] 15.6[29]
Correlation (PhOH)	2.2[b]	7.0[c]	16.1[d]
Theory (PhOH)	-0.3	7.6	26

[a]In toluene. [b]Estimated from eq. S6.5: $\Delta_{HB}G = -10.03\alpha_2^H(\text{PhOH})\beta_2^H(\text{pyr}) + 1.492$, kcal/mol using $\alpha_2^H(\text{PhOH}) = 0.596$ and $\beta_2^H(\text{pyr}) = 0.62$.[32,33] [c]Estimated from eq. S6.3: $\Delta_{HB}H = -20.56\alpha_2^H(\text{PhOH})\beta_2^H(\text{pyr}) + 0.59$, kcal/mol. [d]Derived from $\Delta_{HB}S = (\Delta_{HB}H - \Delta_{HB}G)/T$.

Table S3. Comparison of thermochemistry (in kcal/mol and cal/(mol K) at 298 K) computed with DFT and evaluated from empirical correlations for H-bonding in CCl_4 ($\alpha_2^{\mathrm{H}} = \beta_2^{\mathrm{H}} = 0$) between MeCN ($\beta_2^{\mathrm{H}} = 0.44$) and *p*-substituted phenols: MeOPhOH ($\alpha_2^{\mathrm{H}} = 0.573$), NCPhOH ($\alpha_2^{\mathrm{H}} = 0.787$), and O_2NPhOH ($\alpha_2^{\mathrm{H}} = 0.824$). The correlations used are given by eq. S6.3 and S6.5 (with S = MeCN and $log[\mathrm{MeCN}] = 0$, which accounts for the MeCN solute standard state of 1 M in CCl_4).

Source (R-)	$-\Delta_{\mathrm{HB}}G$	$-\Delta_{\mathrm{HB}}H$	$-\Delta_{\mathrm{HB}}S$
Correlation (MeO-)	1.0[a]	4.6[b]	12[c]
Theory (MeO-)	−1.6	5.1	23
Correlation (NC-)	2.0[a]	6.5[b]	15[c]
Theory (NC-)	0.0	6.8	23
Correlation (O_2N-)	2.1[a]	6.9[b]	16[c]
Theory (O_2N-)	0.4	7.1	23

[a]Estimated from $\Delta_{\mathrm{HB}}G = -10.03\alpha_2^{\mathrm{H}}(\mathrm{PhOH})\beta_2^{\mathrm{H}}(\mathrm{MeCN}) + 1.492$ kcal/mol. [b]Estimated from $\Delta_{\mathrm{HB}}H = -20.56\alpha_2^{\mathrm{H}}(\mathrm{PhOH})\beta_2^{\mathrm{H}}(\mathrm{MeCN}) + 0.59$ kcal/mol. [c]Derived from $\Delta_{\mathrm{HB}}S = (\Delta_{\mathrm{HB}}H - \Delta_{\mathrm{HB}}G)/T$.

Table S4. Computed enthalpies (kcal/mol) for H-bonding of *p*-substituted phenols and trifluoroethanol to **1(T)**, MeCN, and CH_2Cl_2.

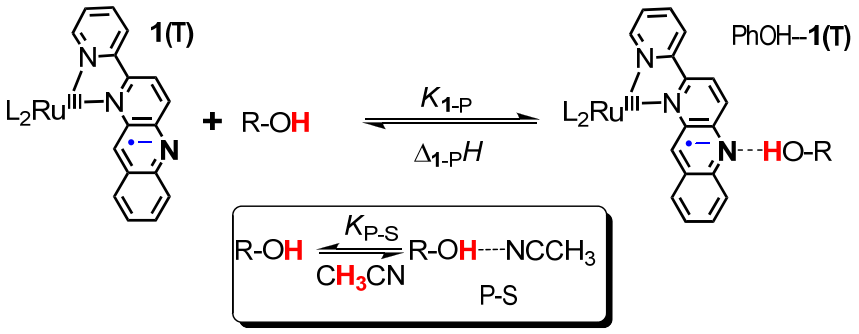

R-	$-\Delta_{1\text{-}P}H$		$-\Delta_{P\text{-}S}H$	
	In MeCN	In CH_2Cl_2	In MeCN	In CH_2Cl_2
MeOPh-	7.2	7.0	3.4	0.8
NCPh-	8.2	7.7	4.1	0.6
O_2NPh-	8.7	7.9	4.3	0.6
CF_3CH_2-	6.9	5.6	2.6	0.4

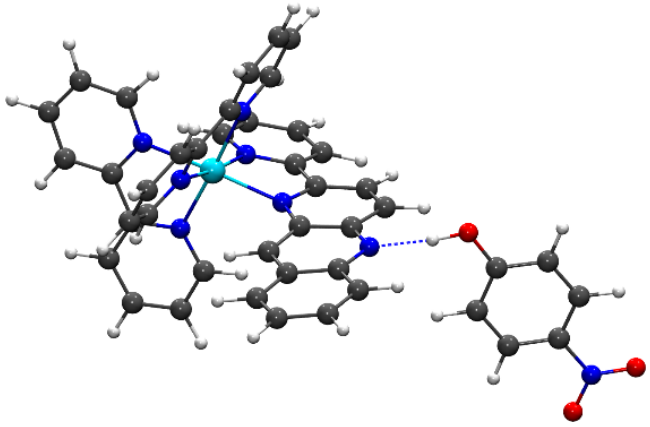

Figure S17. Ball and stick representation of the optimized structure for **1**(**T**) H-bonded to *p*-nitrophenol. The computed hydrogen bond (N–O) distances are 2.74 and 2.76 Å in MeCN and CH_2Cl_2, respectively. For the weaker HB donor, *p*-methoxyphenol, the corresponding distances are longer: 2.80 and 2.81 Å.

Section S8

Materials and Methods

Materials. Acetonitrile (MeCN) and dichloromethane (CH_2Cl_2) both of the HPLC Plus grade (≥99.9%) were purchased from Sigma-Aldrich. Acetonitrile was distilled from potassium borohydride and dried over activated 3Å molecular sieves. Dichloromethane was passed through activated neutral alumina and dried over activated 3Å molecular sieves. *p*-methoxyphenol, *p*-phenylphenol, *p*-chlorophenol, methyl 4-hydroxybenzoate, *p*-cyanophenol and *p*-nitrophenol (all >97% purity) were purchased from Sigma-Aldrich and further purified by sublimation. The deuterated analogs have been prepared by dissolving purified phenols in CH_3OD and removing solvent under vacuum. An isotope enrichment of over 98% was found by NMR in CD_3CN. Ruthenium complexes were prepared according to literature procedures: $[Ru(bpy)_2(pbn)](PF_6)_2$ (**1**; pbn = 2-(2-pyridyl)benzo[*b*]-1,5-naphthyridine, bpy = 2,2′-bipyridine),[34] $[Ru(bpy)_2(i\text{-}pbn)](PF_6)_2$ (**1i**; i-pbn = 3-(pyrid-2′-yl)-4-azaacridine),[13] and $[Ru(bpz)_3][PF_6]_2$ (**3**).[35]

Experimental procedures. All samples were prepared and transferred into a 1 cm path length optical cuvette equipped with an airtight valve under the inert atmosphere of a glovebox. Absorption spectra were measured with an Agilent 8453 diode-array spectrophotometer. The steady-state emission spectra were measured using a PTI fluorimeter. The transient absorption and emission measurements were conducted with temperature stabilization and a 90° beam geometry using a home-built setup controlled by custom LabView software. Excitation was provided either by the second harmonic 532 nm light from a Nd/YAG SpectraPhysics Lab 170 laser in the seeded mode with a pulse width of ~2 ns or by a laser beam from a tunable VersaScan/240/ULD OPO pumped by the Lab 170. The excitation energy was maintained in the 4-7 mJ/pulse range using a half-waveplate and polarizer. A pulsed Xe arc lamp was used as the analyzing light source. A PMT (Hamamatsu, R928) or gated intensified CCD (Princeton

Instruments PI-MAX 1024UNIGEN2) were used as detectors. The integrity of samples during the course of an experiment was verified by comparing their Uv-Vis spectra before and after transient measurements.

References

(1) Concepcion, J. J.; Brennaman, M. K.; Deyton, J. R.; Lebedeva, N. V.; Forbes, M. D. E.; Papanikolas, J. M.; Meyer, T. J. Excited-State Quenching by Proton-Coupled Electron Transfer. *J. Am. Chem. Soc.* **2007**, *129*, 6968-6969.

(2) Bronner, C.; Wenger, O. S. Kinetic Isotope Effects in Reductive Excited-State Quenching of $[Ru(2,2'\text{-bipyrazine})_3]^{2+}$ by Phenols. *J. Phys. Chem. Lett.* **2012**, *3*, 70-74.

(3) Lebedeva, N. V.; Schmidt, R. D.; Concepcion, J. J.; Brennaman, M. K.; Stanton, I. N.; Therien, M. J.; Meyer, T. J.; Forbes, M. D. E. Structural and pH Dependence of Excited State PCET Reactions Involving Reductive Quenching of the MLCT Excited State of $[Ru^{II}(bpy)_2(bpz)]^{2+}$ by Hydroquinones. *J. Phys. Chem. A* **2011**, *115*, 3346-3356.

(4) Rajeswari, A.; Ramdass, A.; Muthu Mareeswaran, P.; Rajagopal, S. Electron Transfer Studies of Ruthenium(II) Complexes with Biologically Important Phenolic Acids and Tyrosine. *J. Fluoresc.* **2016**, *26*, 531-543.

(5) Pizano, A. A.; Yang, J. L.; Nocera, D. G. Photochemical Tyrosine Oxidation with a Hydrogen-Bonded Proton Acceptor by Bidirectional Proton-Coupled Electron Transfer. *Chem. Sci.* **2012**, *3*, 2457-2461.

(6) Chen, J.; Kuss-Petermann, M.; Wenger, O. S. Distance Dependence of Bidirectional Concerted Proton–Electron Transfer in Phenol-$[Ru(2,2'\text{-bipyridine})_3]^{2+}$ Dyads. *Chem. Eur. J.* **2014**, *20*, 4098-4104.

(7) Kuss-Petermann, M.; Wenger, O. S. Photoacid Behavior versus Proton-Coupled Electron Transfer in Phenol–$[Ru(bpy)_3]^{2+}$ Dyads. *J. Phys. Chem. A* **2013**, *117*, 5726-5733.

(8) Rajeswari, A.; Ramdass, A.; Muthu Mareeswaran, P.; Velayudham, M.; Rajagopal, S. Electron Transfer Reactions of Osmium(II) Complexes with Phenols and Phenolic Acids. *J. Mol. Struct.* **2016**, *1115*, 75-84.

(9) Dongare, P.; Bonn, A. G.; Maji, S.; Hammarström, L. Analysis of Hydrogen-Bonding Effects on Excited-State Proton-Coupled Electron Transfer from a Series of Phenols to a Re(I) Polypyridyl Complex. *J. Phys. Chem. C* **2017**, *121*, 12569-12576.

(10) Polyansky, D. E.; Cabelli, D.; Muckerman, J. T.; Fukushima, T.; Tanaka, K.; Fujita, E. Mechanism of Hydride Donor Generation Using a Ru(II) Complex Containing an NAD(+) Model Ligand: Pulse and Steady-State Radiolysis Studies. *Inorg. Chem.* **2008**, *47*, 3958-3968.

(11) Polyansky, D.; Cabelli, D.; Muckerman, J. T.; Fujita, E.; Koizumi, T.; Fukushima, T.; Wada, T.; Tanaka, K. Photochemical and Radiolytic Production of an Organic Hydride Donor with a Ru-II Complex Containing an NAD(+) Model Ligand. *Angew. Chem. Int. Ed.* **2007**, *46*, 4169-4172.

(12) Cohen, B. W.; Polyansky, D. E.; Achord, P.; Cabelli, D.; Muckerman, J. T.; Tanaka, K.; Thummel, R. P.; Zong, R. F.; Fujita, E. Steric Effect for Proton, Hydrogen-Atom, and Hydride Transfer Reactions with Geometric Isomers of NADH-Model Ruthenium Complexes. *Faraday Discuss.* **2012**, *155*, 129-144.

(13) Cohen, B. W.; Polyansky, D. E.; Zong, R. F.; Zhou, H.; Ouk, T.; Cabelli, D. E.; Thummel, R. P.; Fujita, E. Differences of pH-Dependent Mechanisms on Generation of Hydride Donors using Ru(II) Complexes Containing Geometric Isomers of NAD(+) Model Ligands: NMR and Radiolysis Studies in Aqueous Solution. *Inorg. Chem.* **2010**, *49*, 8034-8044.

(14) Mulder, P.; Korth, H.-G.; Pratt, D. A.; DiLabio, G. A.; Valgimigli, L.; Pedulli, G. F.; Ingold, K. U. Critical Re-evaluation of the O−H Bond Dissociation Enthalpy in Phenol. *J. Phys. Chem. A* **2005**, *109*, 2647-2655.

(15) Zhao, Y.; Truhlar, D. G. The M06 Suite of Density Functionals for Main Group Thermochemistry, Thermochemical Kinetics, Noncovalent Interactions, Excited States, and Transition

Elements: Two New Functionals and Systematic Testing of Four M06-Class Functionals and 12 Other Functionals. *Theor. Chem. Acc.* **2008**, *120*, 215-241.

(16) Zhao, Y.; Truhlar, D. G. Density Functionals with Broad Applicability in Chemistry. *Acc. Chem. Res.* **2008**, *41*, 157-167.

(17) Zhao, Y.; Truhlar, D. G. The Minnesota Density Functionals and their Applications to Problems in Mineralogy and Geochemistry. *Rev. Mineral. Geochem.* **2010**, *71*, 19-37.

(18) Marenich, A. V.; Cramer, C. J.; Truhlar, D. G. Universal Solvation Model Based on Solute Electron Density and on a Continuum Model of the Solvent Defined by the Bulk Dielectric Constant and Atomic Surface Tensions. *J. Phys. Chem. B* **2009**, *113*, 6378-6396.

(19) Andrae, D.; Haussermann, U.; Dolg, M.; Stoll, H.; Preuss, H. Energy-Adjusted Abinitio Pseudopotentials for the 2nd and 3rd Row Transition-Elements. *Theor. Chim. Acta* **1990**, *77*, 123-141.

(20) Hehre, W. J.; Radom, L.; Schleyer, P. v. R.; Pople, J. A. *Ab Initio Molecular Orbital Theory*; Wiley: New York, 1986.

(21) Frisch, M. J.; Trucks, G. W.; Schlegel, H. B.; Scuseria, G. E.; Robb, M. A.; Cheeseman, J. R.; Scalmani, G.; Barone, V.; Mennucci, B.; Petersson, G. A.; Nakatsuji, H.; Caricato, M.; Li, X.; Hratchian, H. P.; Izmaylov, A. F.; Bloino, J.; Zheng, G.; Sonnenberg, J. L.; Hada, M.; Ehara, M.; Toyota, K.; Fukuda, R.; Hasegawa, J.; Ishida, M.; Nakajima, T.; Honda, Y.; Kitao, O.; Nakai, H.; Vreven, T.; Montgomery, J. A.; Peralta, J. E.; Ogliaro, F.; Bearpark, M.; Heyd, J. J.; Brothers, E.; Kudin, K. N.; Staroverov, V. N.; Kobayashi, R.; Normand, J.; Raghavachari, K.; Rendell, A.; Burant, J. C.; Iyengar, S. S.; Tomasi, J.; Cossi, M.; Rega, N.; Millam, J. M.; Klene, M.; Knox, J. E.; Cross, J. B.; Bakken, V.; Adamo, C.; Jaramillo, J.; Gomperts, R.; Stratmann, R. E.; Yazyev, O.; Austin, A. J.; Cammi, R.; Pomelli, C.; Ochterski, J. W.; Martin, R. L.; Morokuma, K.; Zakrzewski, V. G.; Voth, G. A.; Salvador, P.; Dannenberg, J. J.; Dapprich, S.; Daniels, A. D.; Farkas, Ö.; Foresman, J. B.; Ortiz, J. V.; Cioslowski, J.; Fox, D. J. *Gaussian 09, Revision A.02*; Gaussian, Inc.: Wallingford, CT, 2010.

(22) Cramer, C. J. *Essentials of Computational Chemistry: Theories and Models*; 2nd ed.; John Wiley & Sons: Chichester, 2004.

(23) Weigend, F.; Ahlrichs, R. Balanced Basis Sets of Split Valence, Triple Zeta Valence and Quadruple Zeta Valence Quality for H to Rn: Design and Assessment of Accuracy. *Phys. Chem. Chem. Phys.* **2005**, *7*, 3297-3305.

(24) Arnett, E. M.; Joris, L.; Mitchell, E.; Murty, T. S. S. R.; Gorrie, T. M.; Schleyer, P. v. R. Studies of Hydrogen-Bonded Complex Formation. III. Thermodynamics of Complexing by Infrared Spectroscopy and Calorimetry. *J. Am. Chem. Soc.* **1970**, *92*, 2365-2377.

(25) Singh, S.; Rao, C. N. R. Deuterium Isotope Effects on Hydrogen Bonding. *Can. J. Chem.* **1966**, *44*, 2611-&.

(26) Rubin, J.; Panson, G. S. Hydrogen Bonding. II. Phenol Interactions with Substituted Pyridines. *J. Phys. Chem.* **1965**, *69*, 3089-3091.

(27) Mendel, J.; Mogel, A.; Kolbe, A. The Association between Tertiary Amines and Several Alcohols. *Adv. Mol. Relax. Int. Pr.* **1977**, *11*, 9-19.

(28) Aksnes, G.; Gramstad, T. Intermolecular Hydrogen Bond Association between Phenol and Organophosphorus Compounds. *Acta Chem. Scand.* **1960**, *14*, 1485-1494.

(29) Gramstad, T. Studies of Hydrogen Bonding 3. Intermolecular Hydrogen Bond Association between Nitrogen Compounds and Methanol, Phenol, Alpha-Napththol and Pentachlorophenol. *Acta Chem. Scand.* **1962**, *16*, 807-819.

(30) Kolbe, A. Calorimetry in Systems with Hydrogen Bonds. *Z. Phys. Chem.* **1968**, *58*, 75-86.

(31) Rospenk, M.; Zeegers-Huyskens, T. FT-IR (7500−1800 cm-1) Study of Hydrogen-Bond Complexes between Phenols−OH(OD) and Pyridine. Evidence of Proton Transfer in the Second Vibrational Excited State. *J. Phys. Chem. A* **1997**, *101*, 8428-8434.

(32) Abraham, M. H.; Grellier, P. L.; Prior, D. V.; Duce, P. P.; Morris, J. J.; Taylor, P. J. Hydrogen-Bonding 7. A Scale of Solute Hydrogen-Bond Acidity Based on Log K-Values for Complexation in Tetrachloromethane. *J. Chem. Soc., Perkin Trans. 2* **1989**, 699-711.

(33) Abraham, M. H.; Grellier, P. L.; Prior, D. V.; Morris, J. J.; Taylor, P. J. Hydrogen-Bonding 10. A Scale of Solute Hydrogen-Bond Basicity Using Log K Values for Complexation in Tetrachloromethane. *J. Chem. Soc., Perkin Trans. 2* **1990**, 521-529.

(34) Koizumi, T.; Tanaka, K. Reversible Hydride Generation and Release from the Ligand of $Ru(pbn)(bpy)_2$ $(PF6)_2$ Driven by a pbn-Localized Redox Reaction. *Angew. Chem. Int. Ed.* **2005**, *44*, 5891-5894.

(35) Rillema, D. P.; Allen, G.; Meyer, T. J.; Conrad, D. Redox Properties of Ruthenium(II) Tris Chelate Complexes Containing the Ligands 2,2'-Bipyrazine, 2,2'-Bipyridine, and 2,2'-Bipyrimidine. *Inorg. Chem.* **1983**, *22*, 1617-1622.